

Remote Sensing for the derivation of the mixing-layer height and detection of low-level jets

Stefan Emeis
stefan.emeis@kit.edu

INSTITUTE OF METEOROLOGY AND CLIMATE RESEARCH, Atmospheric Environmental Research



Introduction

- **definition of mixing layer**
- **definition of low-level jets**
- **remote sensing techniques
and results**

Mixing-layer height

Inversion height

literally: inversion in the temperature profile, increase of temperature with height, strong decrease of moisture, radiation inversions, sinking inversions, surface inversions, lifted inversions

Mixing-layer height

(mixing height, mixed-layer height)

upper boundary for vertical exchange (mixing), upper boundary of the well-mixed layer, entrainment, defined by the turbulence profile or by the vertical distribution of a tracer (aerosol, pot. temperature)

Boundary layer height

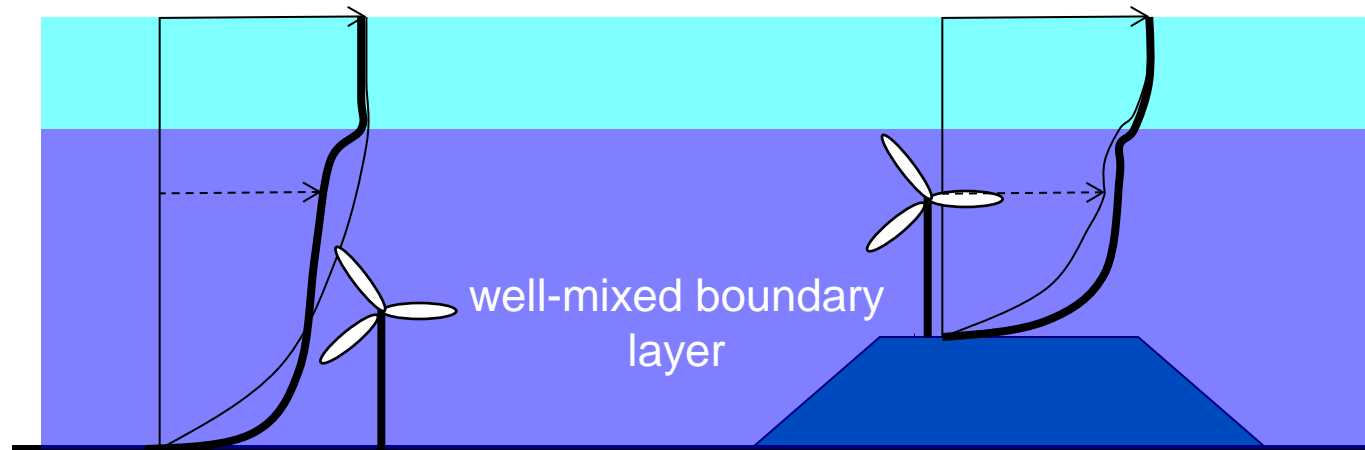
SBL: at night, height of the near-surface layer influenced by surface friction
CBL: at day, height of convective plumes

boundary layer height \approx mixing-layer height

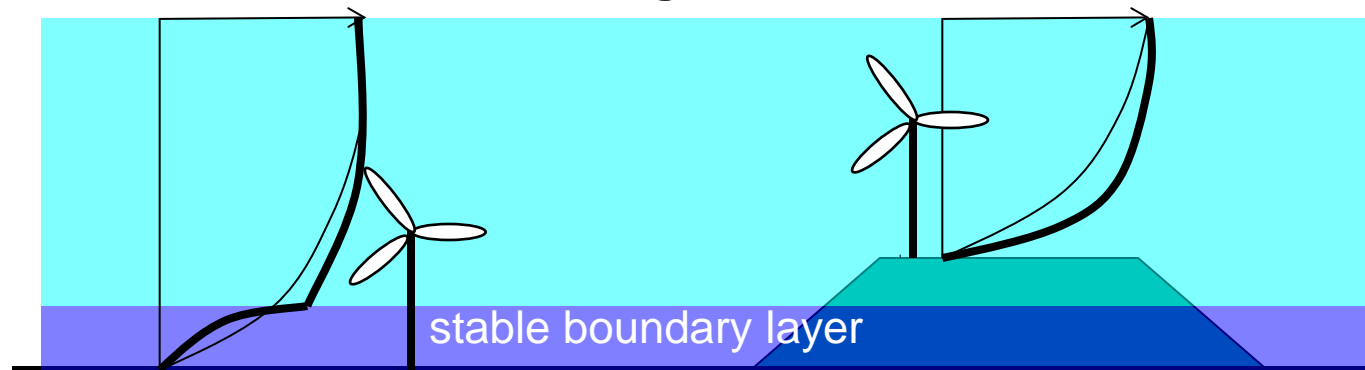
boundary layer height \geq inversion height

Mixing-layer height influences diurnal variation of vertical wind profiles

Day



Night



Relevance for wind energy

The vertical wind profile (equilibrium conditions)

logarithmic law

(with stability correction) $u(z) = (u_*/\kappa) (\ln(z/z_0) - \psi(z/L_*))$

power law

$$u(z) = u(z_A) (z/z_A)^n$$

New proposal
(Gryning et al. 2007)

$$u(z) = \frac{u_{*0}}{\kappa} \left(\ln \left(\frac{z}{z_0} \right) + \frac{z}{L_{MBL,N}} - \frac{z}{z_i} \left(\frac{z}{2L_{MBL,N}} \right) \right)$$

needs information on the PBL or mixing-layer height

Gryning, S.-E., E. Batchvarova, B. Brümmer, H. Jørgensen, S. Larsen, 2007: On the extension of the wind profile over homogeneous terrain beyond the surface boundary layer. *Bound.-Lay. Meteorol.*, **124**, 251–268.

Peña, A., S.-E. Gryning, C.B. Hasager, 2010: Comparing mixing-length models of the diabatic wind profile over homogeneous terrain. *Theor. Appl. Climatol.*, **100**, 325-353.

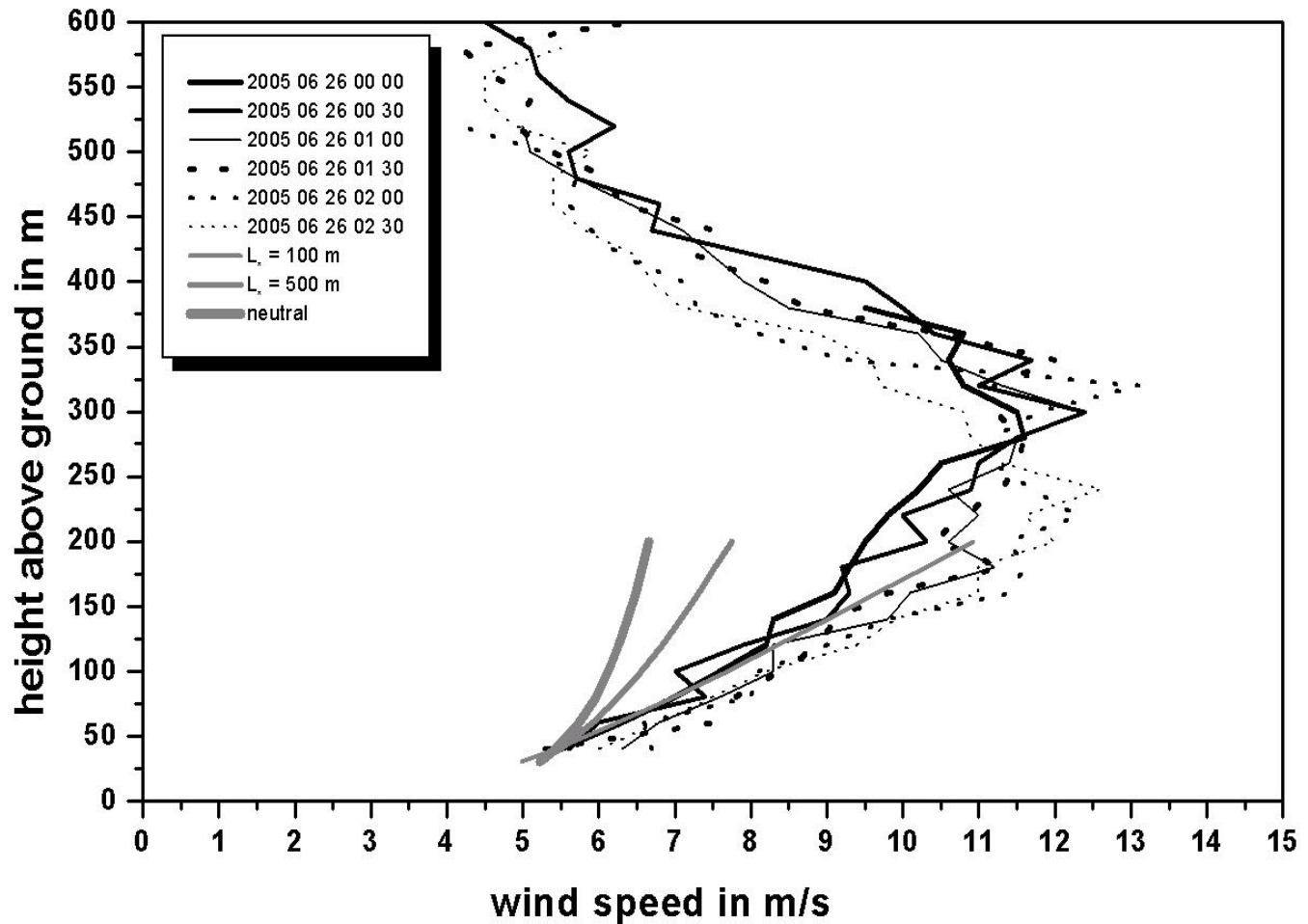
LLJ can only be described by time-dependent equations!

Low-level jet

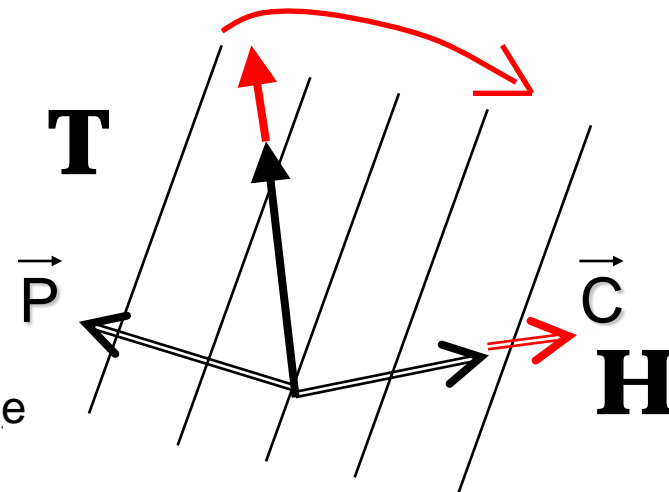
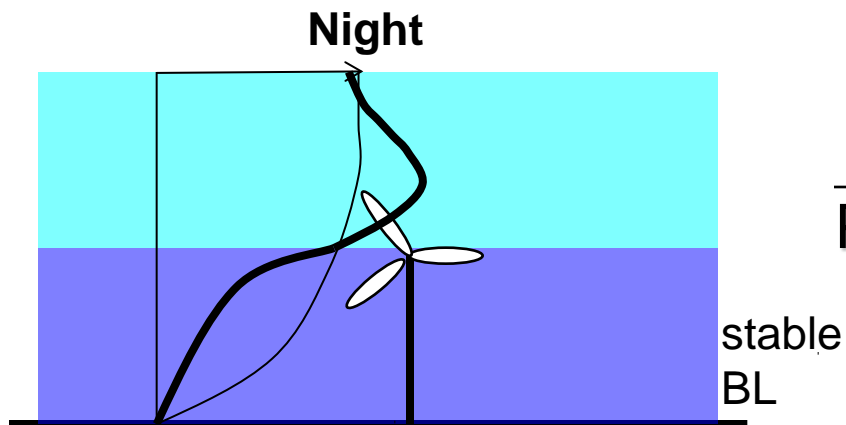
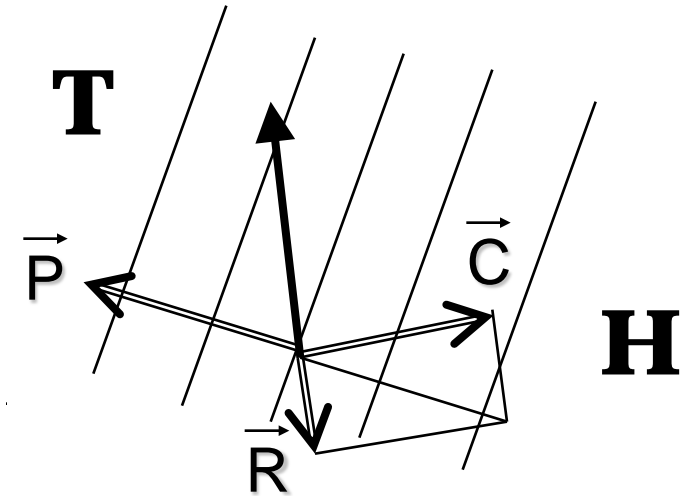
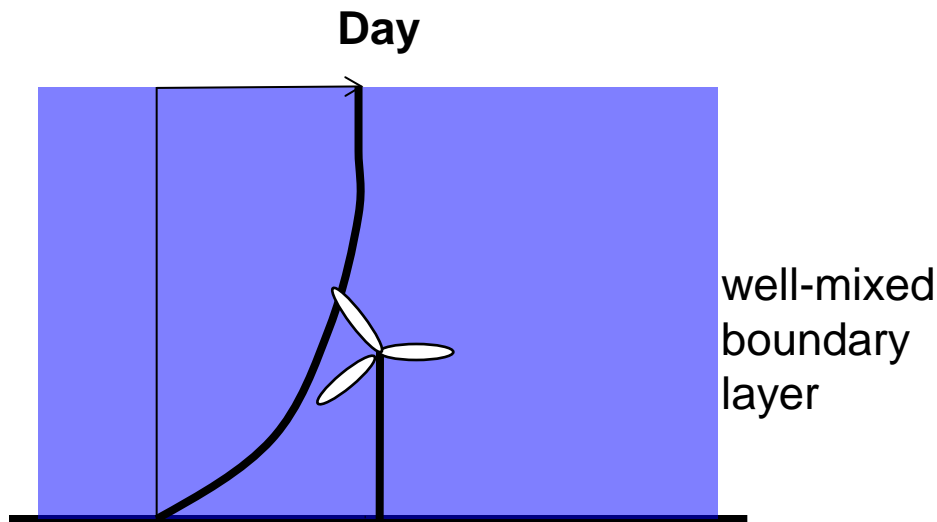
vertical profiles
of wind speed

26 June 2005

AdP Ch d G



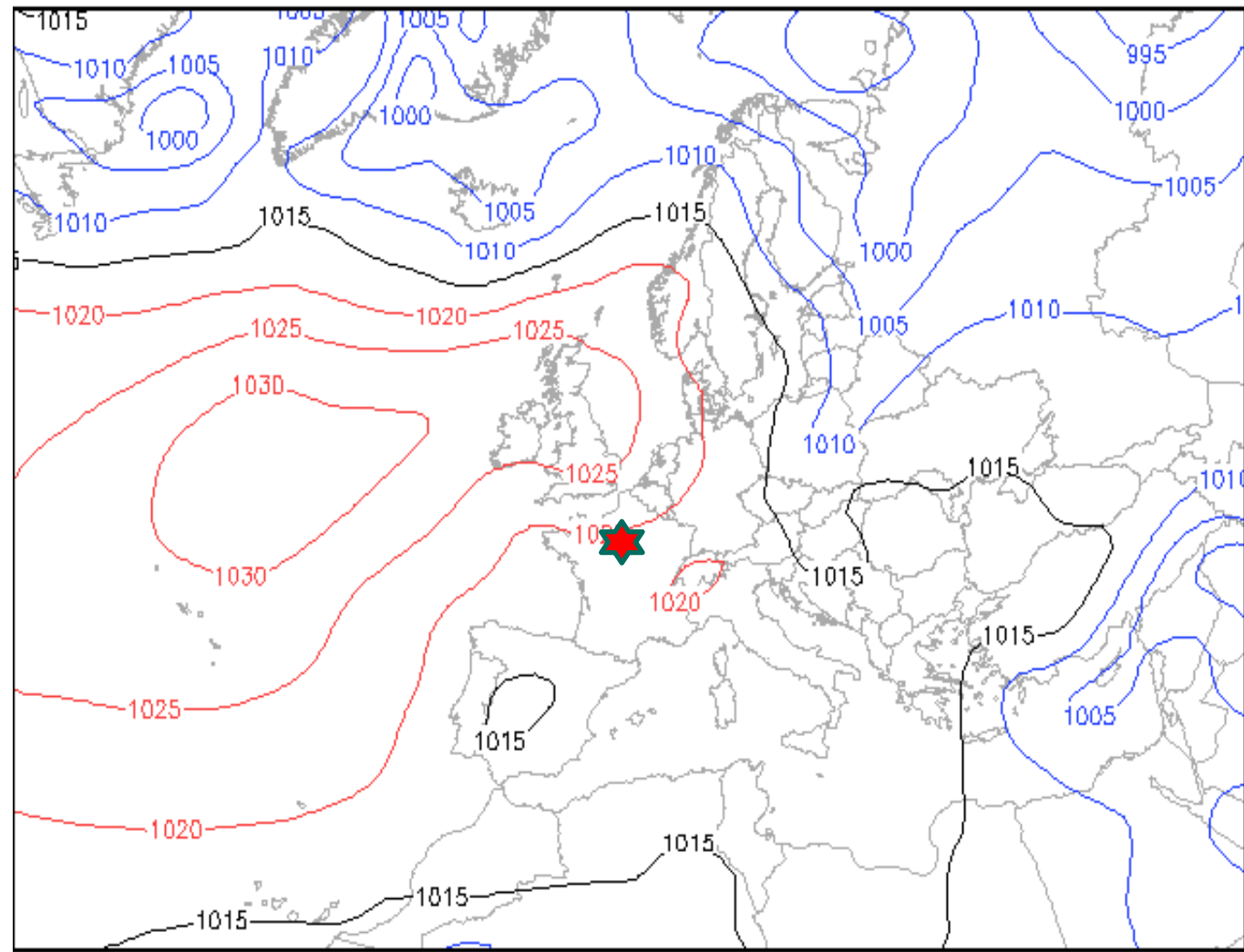
Nocturnal low-level jet and the turning of wind direction with height



**surface pressure
00 GMT**

26 June 2005

**asterisk denotes
location where
LLJ was observed**



Bodendruck GFS (hPa)

So 26.06.05 00 GMT (Sa 00 + 24)

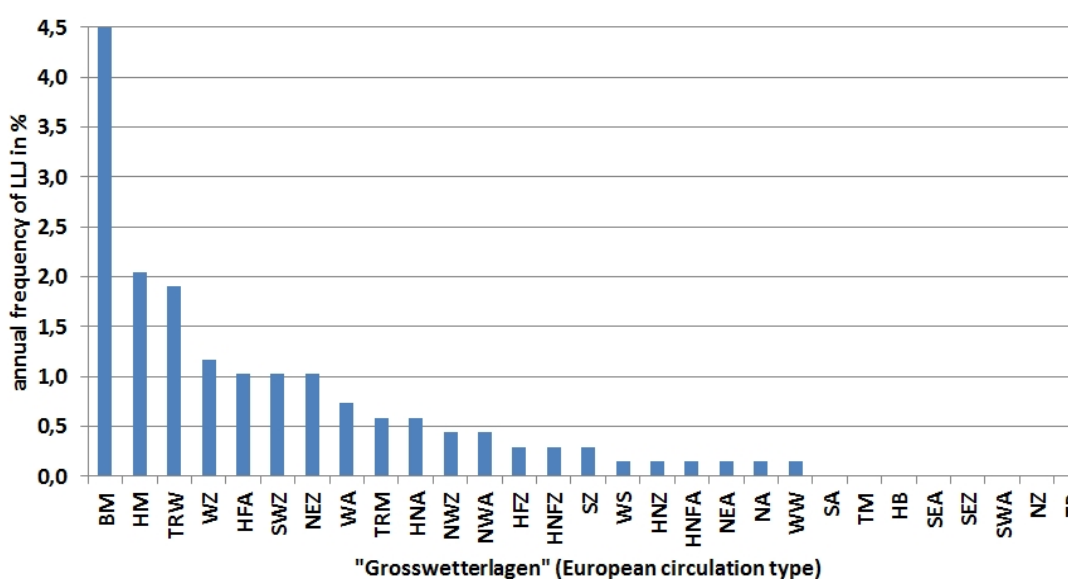
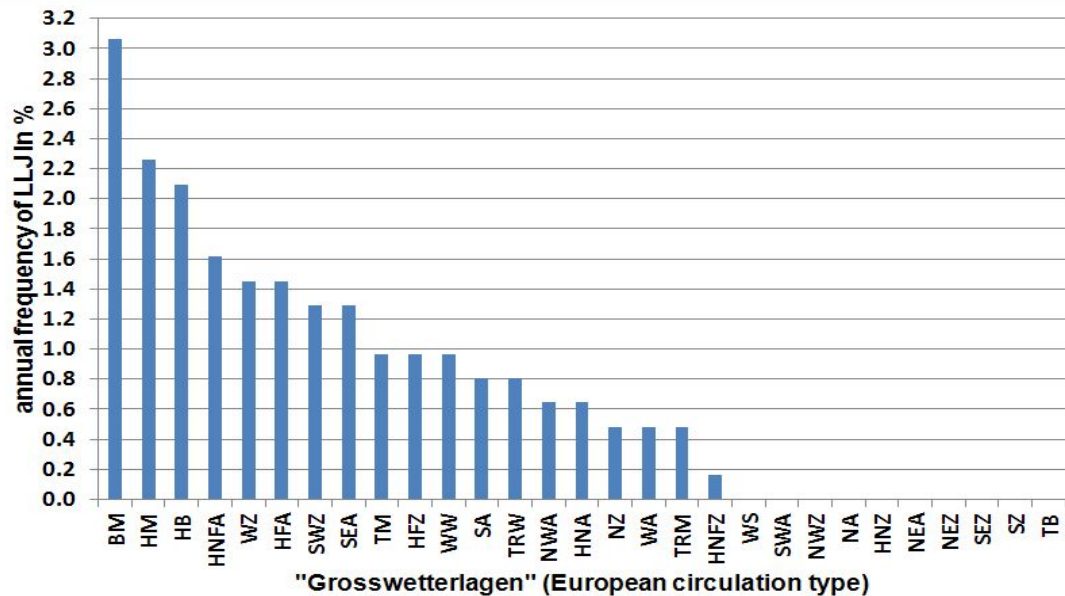
WetterOnline

frequency of LLJ over Hannover
for 20 months in the years
2001 to 2003

roughly 22 % of all nights

over Augsburg in the years
2008-2010, 2014

roughly 17,5 % of all nights



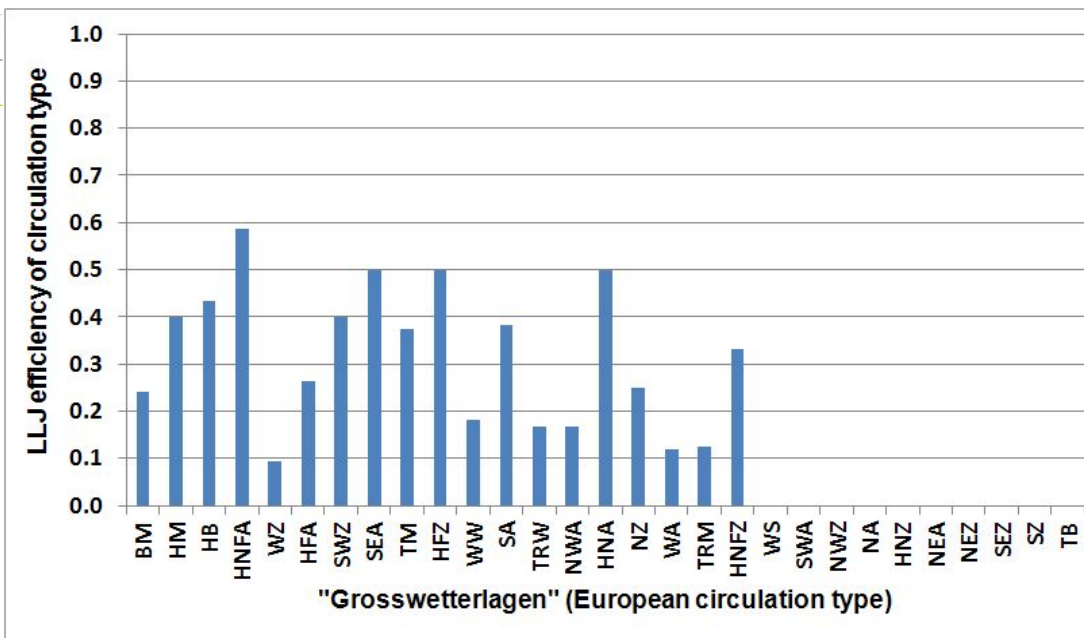
Circulation types:

BM bridge Central Europe
HB high Brit. Isles
HM high Central Europe

...

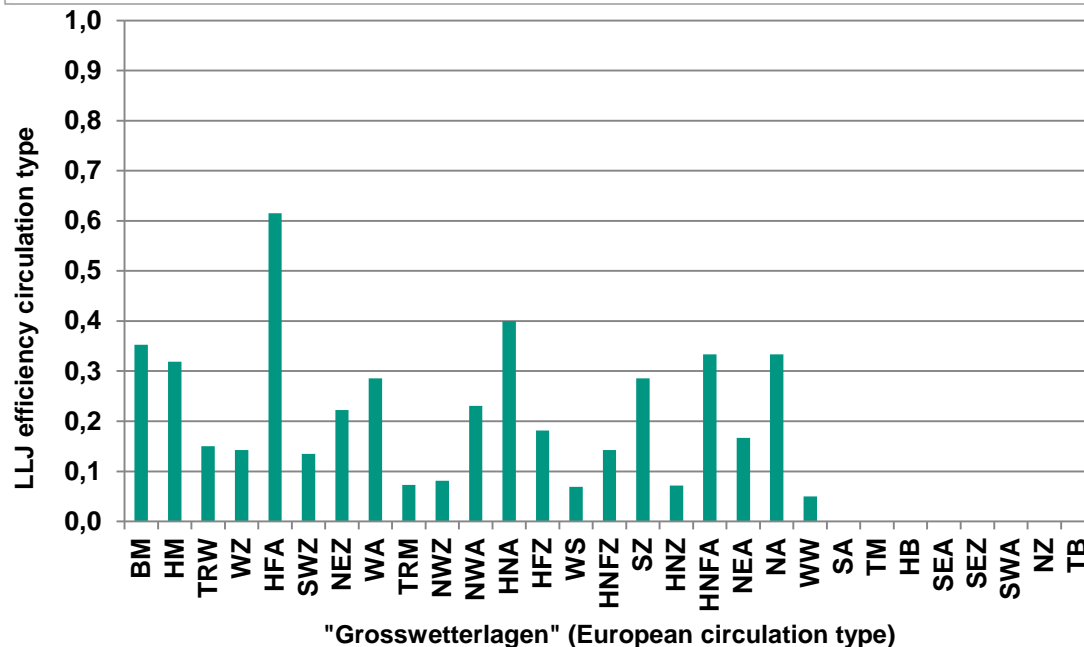
HFA/HFZ high Scandinavia
HNFA high Northern Atlantic

...



“effectivity” for forming a low-level jet

top: Hannover
bottom: Augsburg



Circulation types:

BM bridge Central Europe
HB high Brit. Isles
HM high Central Europe

...

HFA/HFZ high Scandinavia
HNFA high Northern Atlantic

...

Remote sensing of mixing-layer height and low-level jets

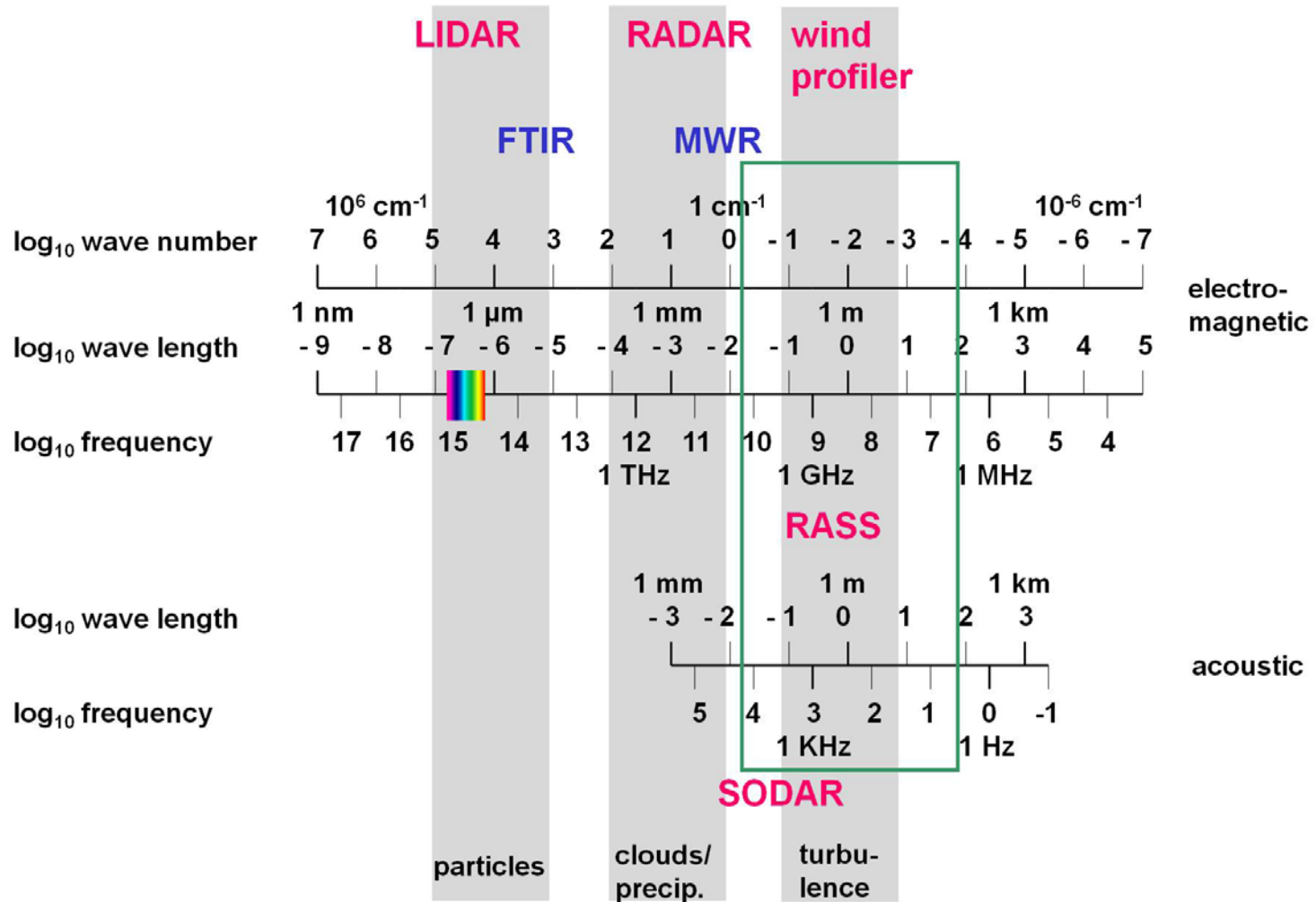
Basic remote sensing techniques

name	principle	spatial resolution	direction	type
RADAR	backscatter, electro-magnetic pulses, fixed wave length	profiling	scanning, slanted	active, monostatic
SODAR	backscatter, acoustic pulses, fixed wave length	profiling	fixed, slanted, vertical	active, usually monostatic
LIDAR ceilometer	backscatter, optical pulses, fixed wave length(s)	profiling	scanning, fixed, horizontal, slanted, vertical	active, monostatic
RASS	backscatter, acoustic, electro-magnetic, fixed wave length	profiling	fixed, vertical	active, monostatic
	absorption, infrared, spectrum	path-averaging	fixed, horizontal, slanted	active, bistatic or passive
FTIR	emission, infrared, spectrum	path-averaging	fixed, horizontal, slanted	passive
DOAS	absorption, optical, fixed wave lengths	path-averaging	fixed, horizontal	active, bistatic
radiometry	electro-magnetic, fixed wave length(s)	averaging, profiling	fixed, scanning, slanted, vertical	passive
tomography	travel time, acoustic, fixed wave length	horizontal distribution	fixed, horizontal	active, multiple emitters and receivers

subject of this lecture

subject of this lecture

Frequencies for atmospheric remote sensing



Emeis, S., 2010: Measurement Methods in Atmospheric Sciences - In situ and remote. Borntraeger, Stuttgart, 272 pp., 103 figs, 28 tables, ISBN 978-3-443-01066-9.

at IMK-IFU

SODAR (Large system),
acoustic backscatter, Doppler
shift analysis → wind, turbulence



SODAR-RASS (Doppler-RASS), acoustic,
electro-magnetic backscatter, determines speed
of sound → wind and temperature profiles



Ceilometer,
backscatter, optical
pulses, wave
length $\sim 0.9 \mu\text{m}$
→ aerosol profiles

Wind-LIDAR, optical backscatter, Doppler shift
analysis, wave length $\sim 1.5 \mu\text{m}$ → wind and
aerosol profiles



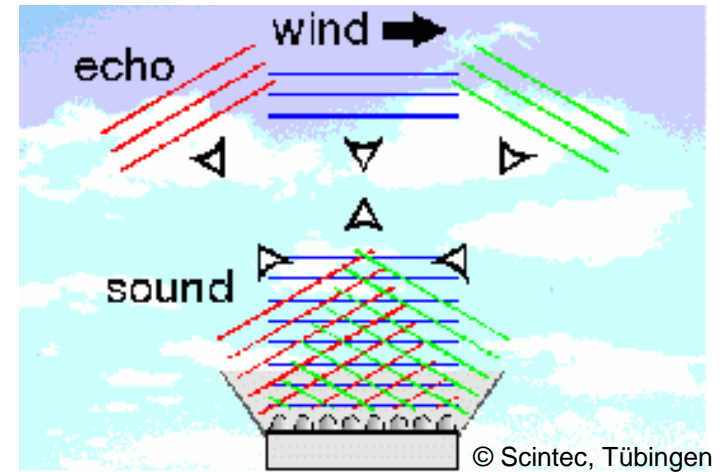
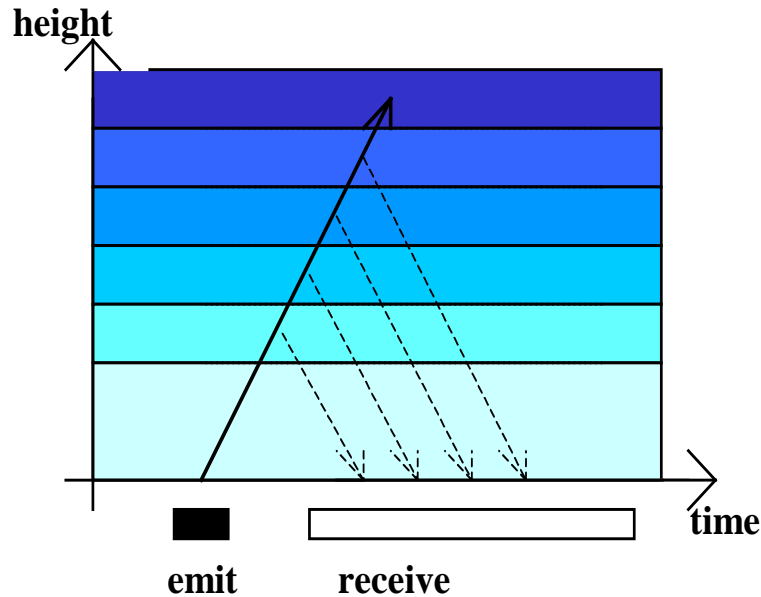
image:
Halo Photonics

SODAR

**algorithms for the determination of
mixing-layer height**

and low-level jet observations

monostatic SODAR: measuring principles



deduction:

sound travel time	=	height
backscatter intensity	=	turbulence
Doppler-shift	=	wind speed

Emission of sound waves
into three directions:

in order to measure all three
components of the wind
(horizontal and vertical)

The SODAR equation:

$$P_R = r^2 (c_s \tau A \varepsilon / 2) P_0 \beta_s e^{-2\sigma r} + P_{bg}$$

P_R received power,

P_0 emitted power,

ε antenna efficiency,

A effective antenna area,

σ sound absorption in air due to classical and molecular absorption due to the collision of water molecules with the oxygen and nitrogen molecules of the air,

r distance between the scattering volume and the instrument,

τ pulse duration (typically between 20 and 100 ms),

β_s backscattering cross-section (typically in the order of $10^{-11} \text{ m}^{-1} \text{ sr}^{-1}$),

c_s sound speed,

P_{bg} background noise.

Emitted power: $\sim 10^3 \text{ W}$, received (backscattered) power: 10^{-15} W

The SODAR equation:

$$P_R = r^2 (c_s \tau A \epsilon / 2) P_0 \beta_s e^{-2\sigma r} + P_{bg}$$

The ratio of the two terms on the right-hand side of the SODAR equation is called signal-to-noise ratio (usually abbreviated as SNR).

The backscattering cross-section β_s is a function of the temperature structure function C_T^2 (Tatarskii 1961).

For a monostatic SODAR we find (Reitebuch 1999) when using the wave number $k = 2\pi/\lambda$:

$$\beta_s(180^\circ) = 0,00408 k^{1/3} C_T^2 / T^2$$

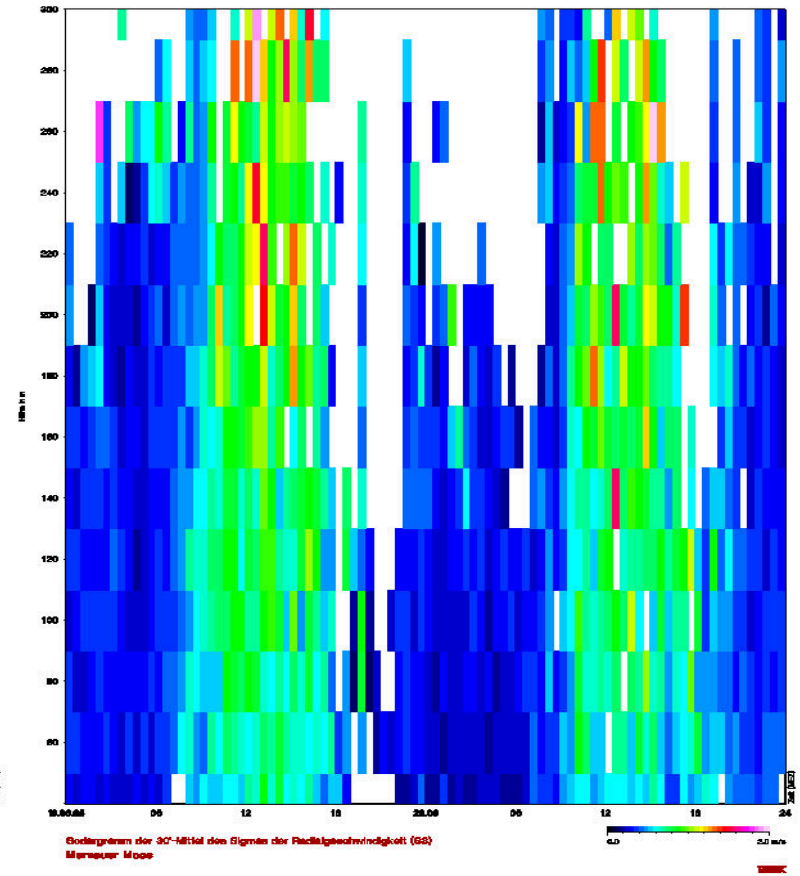
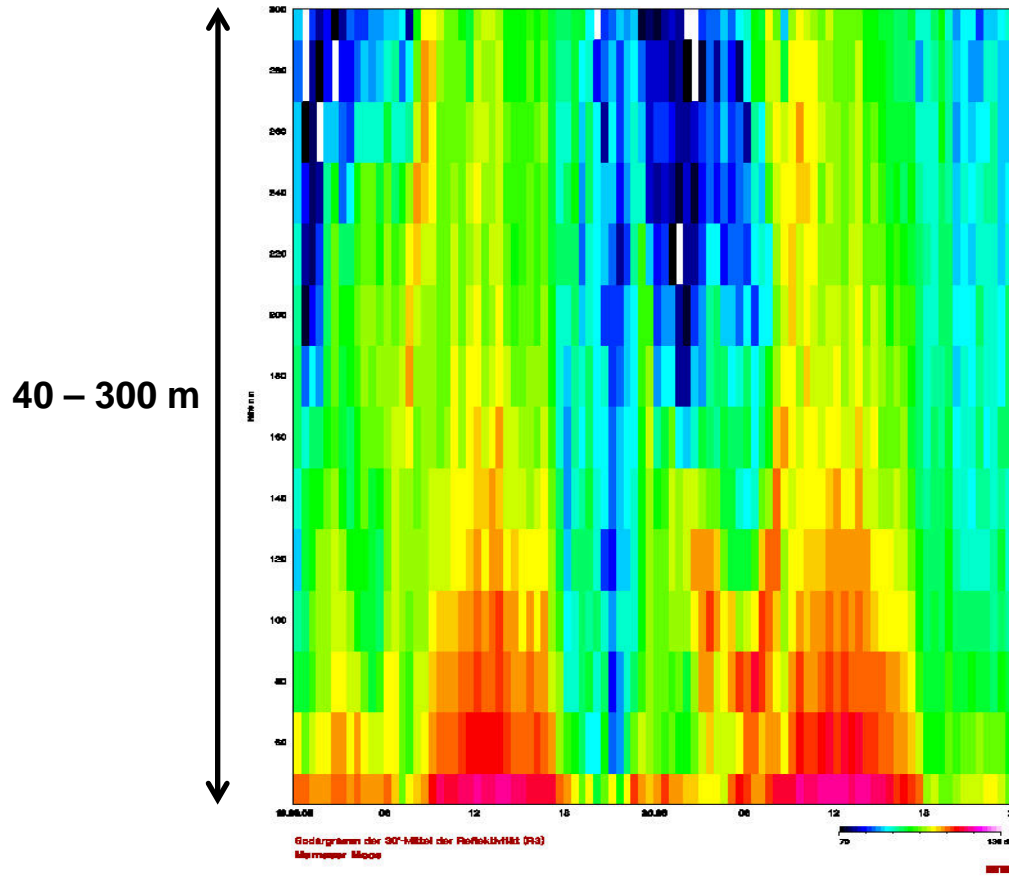
Reitebuch, O., 1999: SODAR-Signalverarbeitung von Einzelpulsen zur Bestimmung hochaufgelöster Windprofile. Schriftenreihe des Fraunhofer-Instituts für Atmosphärische Umweltforschung, Shaker Verlag GmbH Aachen, Bd. 62, 178 S.

Tatarskii, V.I., 1971: The effect of the turbulent atmosphere on wave propagation. Kefer Press, Jerusalem, 472 S.

SODAR sample plot (daytime convective BL)

acoustic backscatter intensity

sigma w

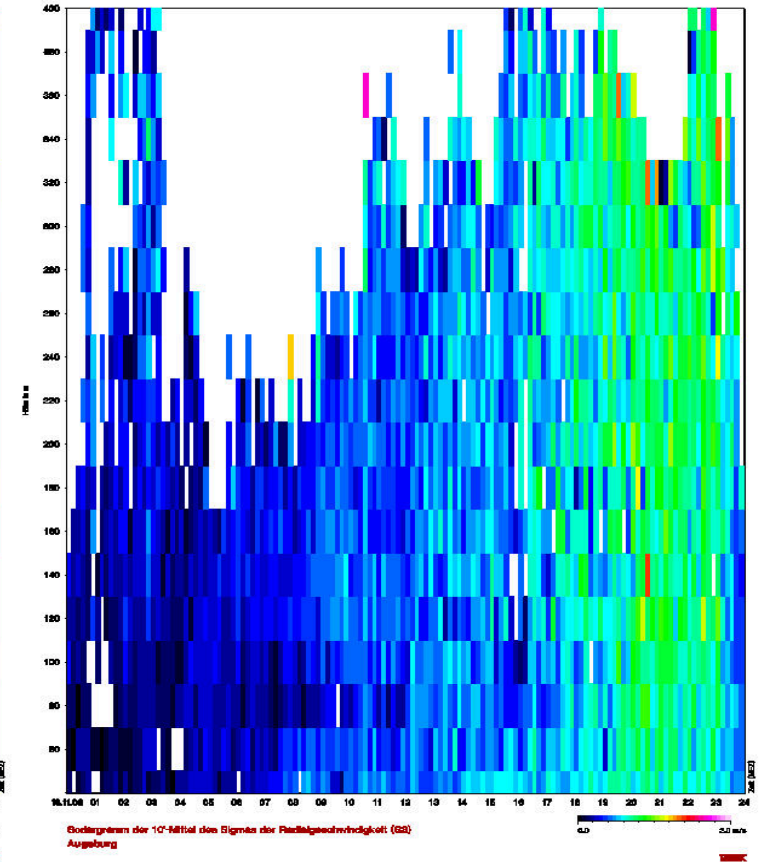
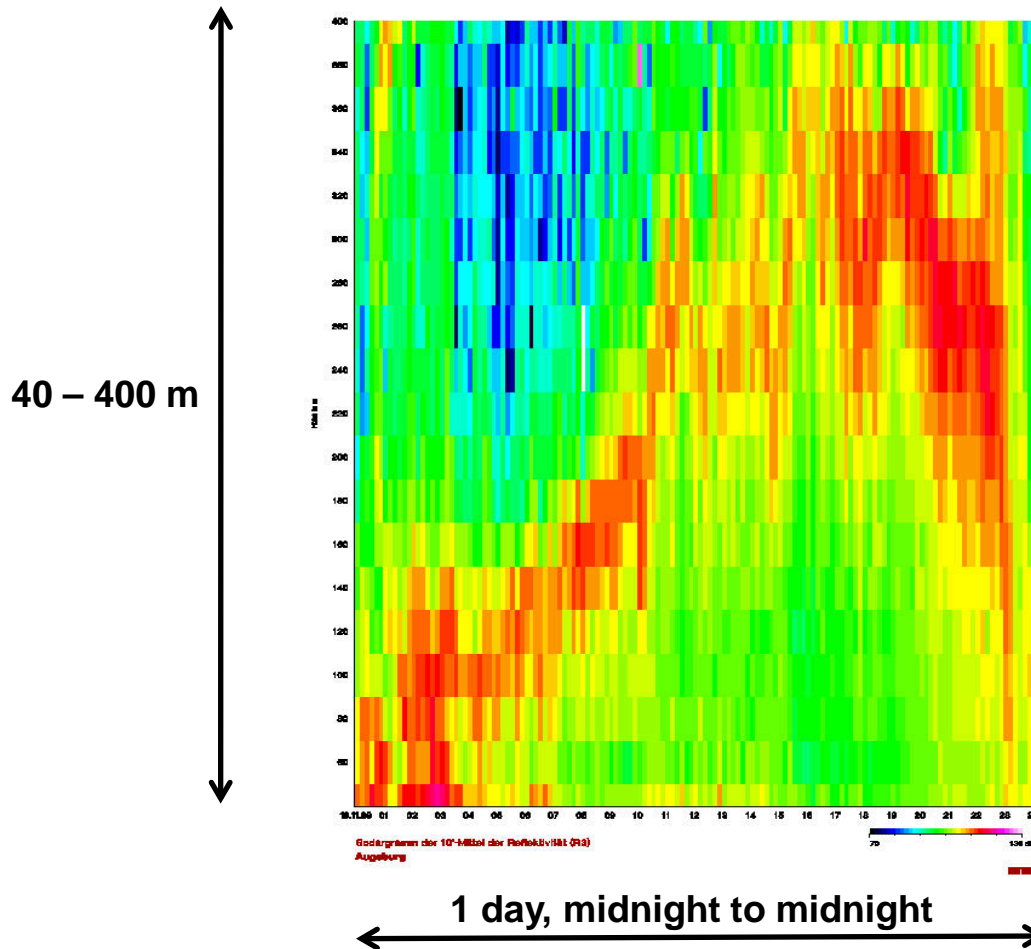


2 days, midnight to midnight

SODAR sample plot (lifted inversion)

acoustic backscatter intensity

sigma w

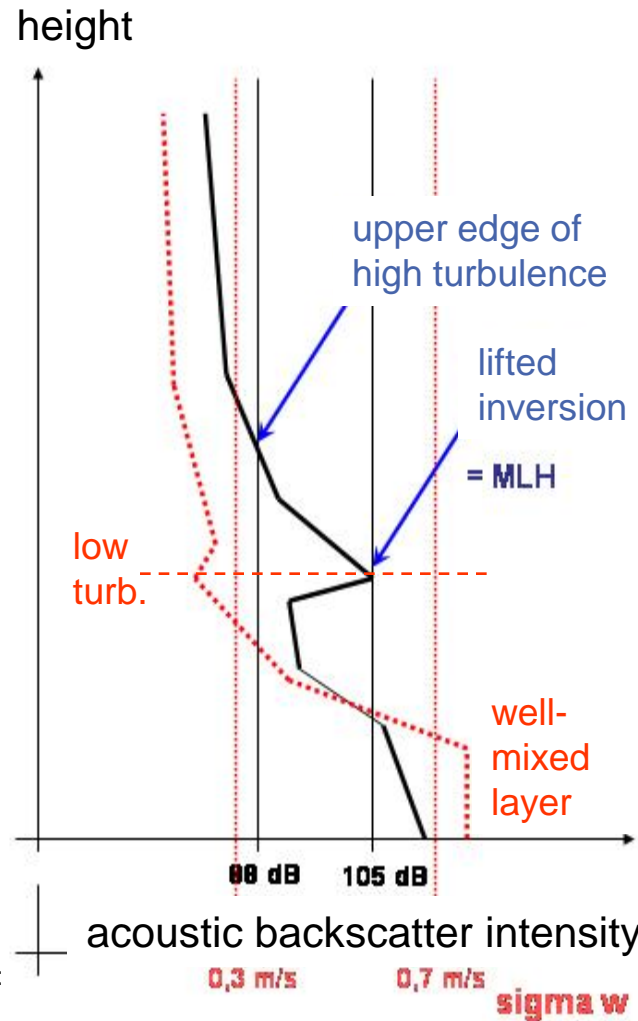


Algorithms to detect MLH from SODAR data

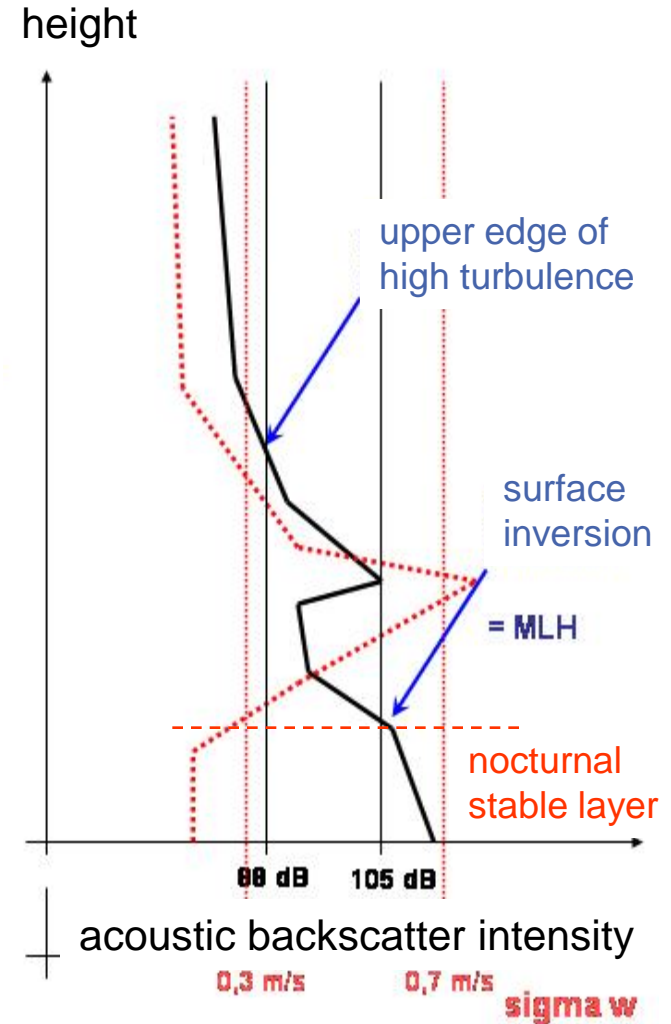
criterion 1:
 upper edge
 of high
 turbulence

criterion 2:
 surface and
 lifted
 inversions

MLH = Min (C1, C2)



example 1: daytime



example 2: night-time

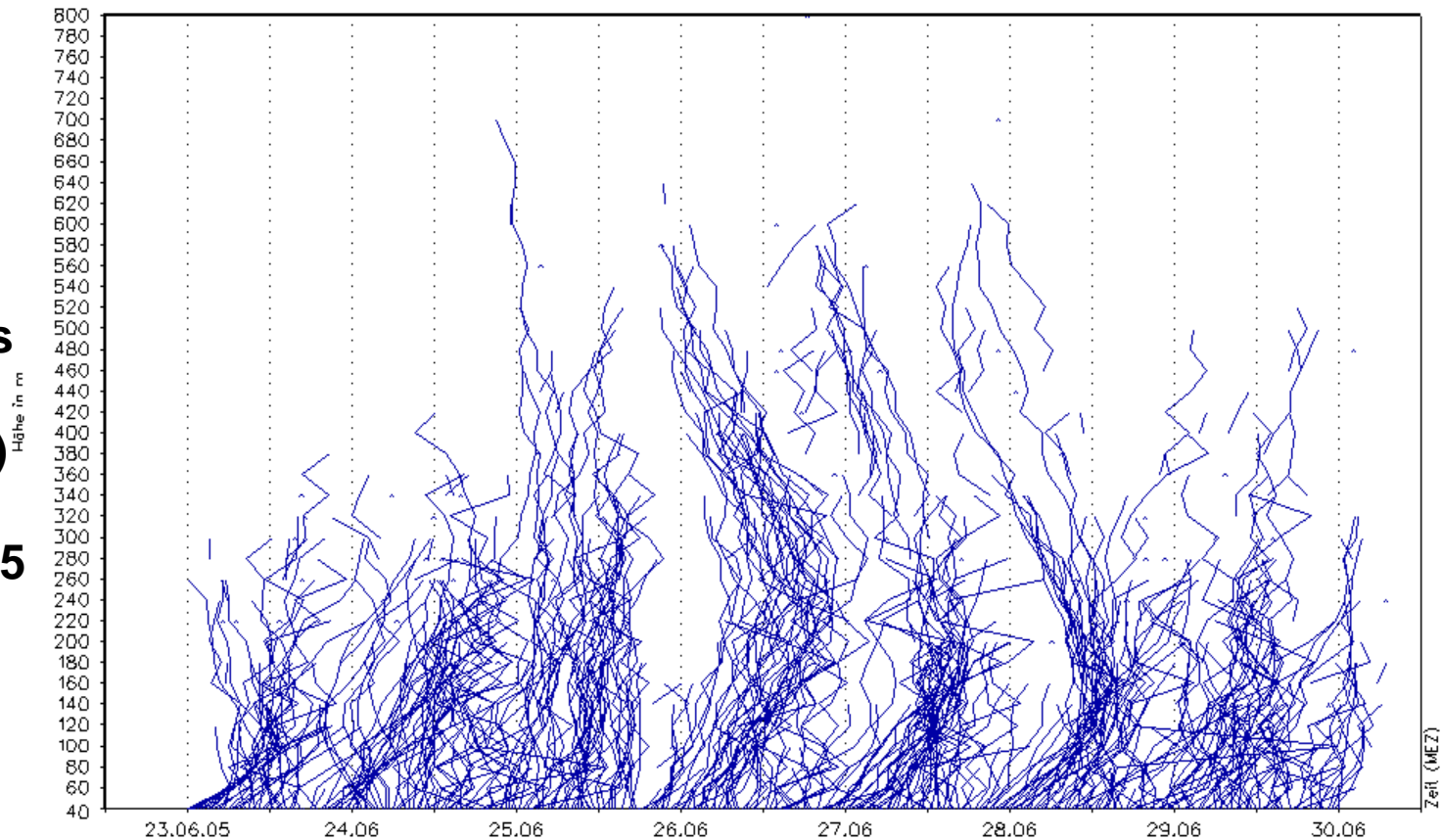
Emeis, S., K. Schäfer, C. Münkel, 2008:
 Surface-based remote sensing of the
 mixing-layer height – a review.
 Meteorol. Z., 17, 621-630.

examples for low-level jet observations with SODAR

vertical profiles
of wind speed
(30 min means)

23-30 June 2005

AdP Ch d G



30'-Mittel der Windgeschwindigkeit (V)
vertical wind profiles

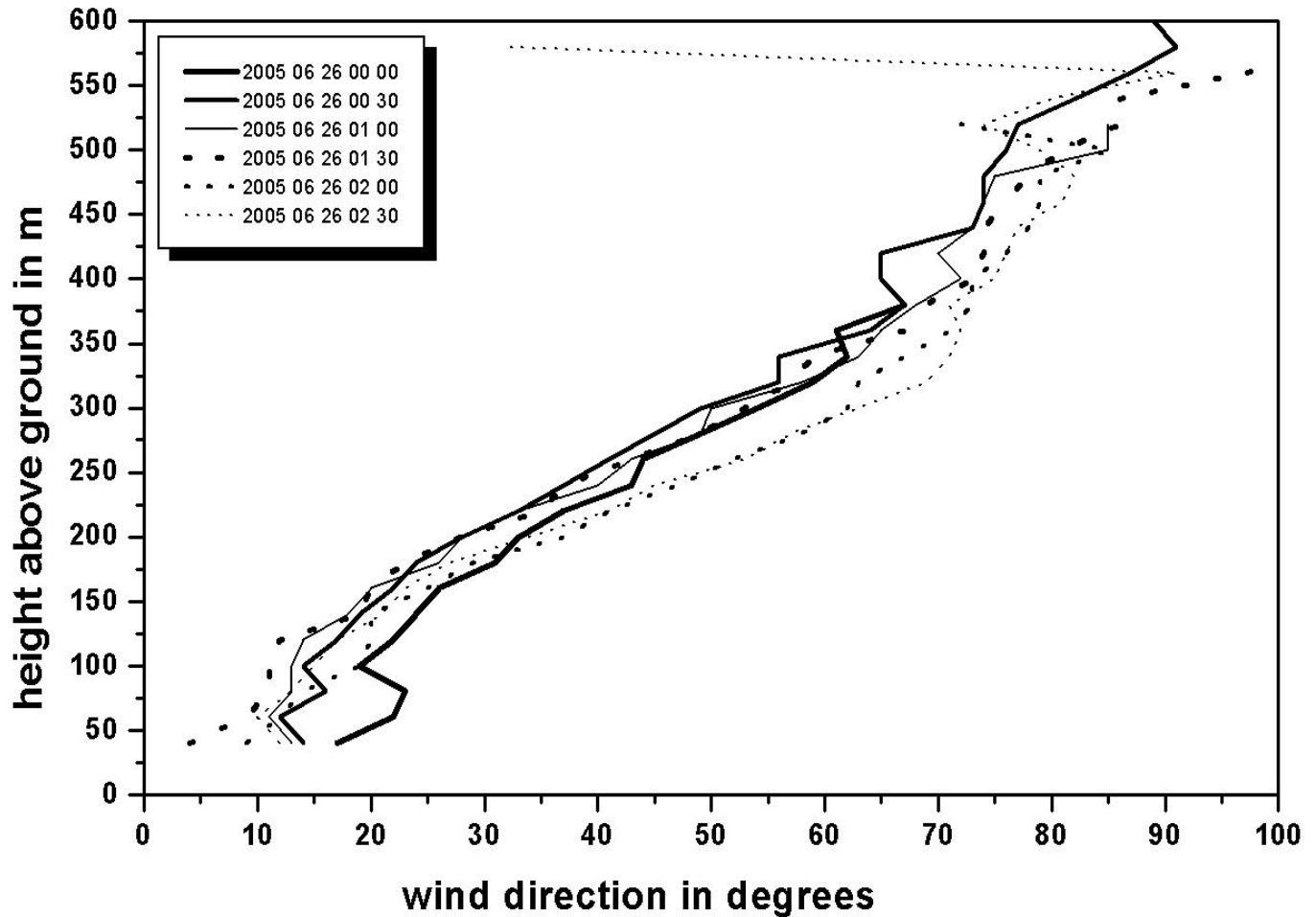
ΔV = 4 m/s

METEK

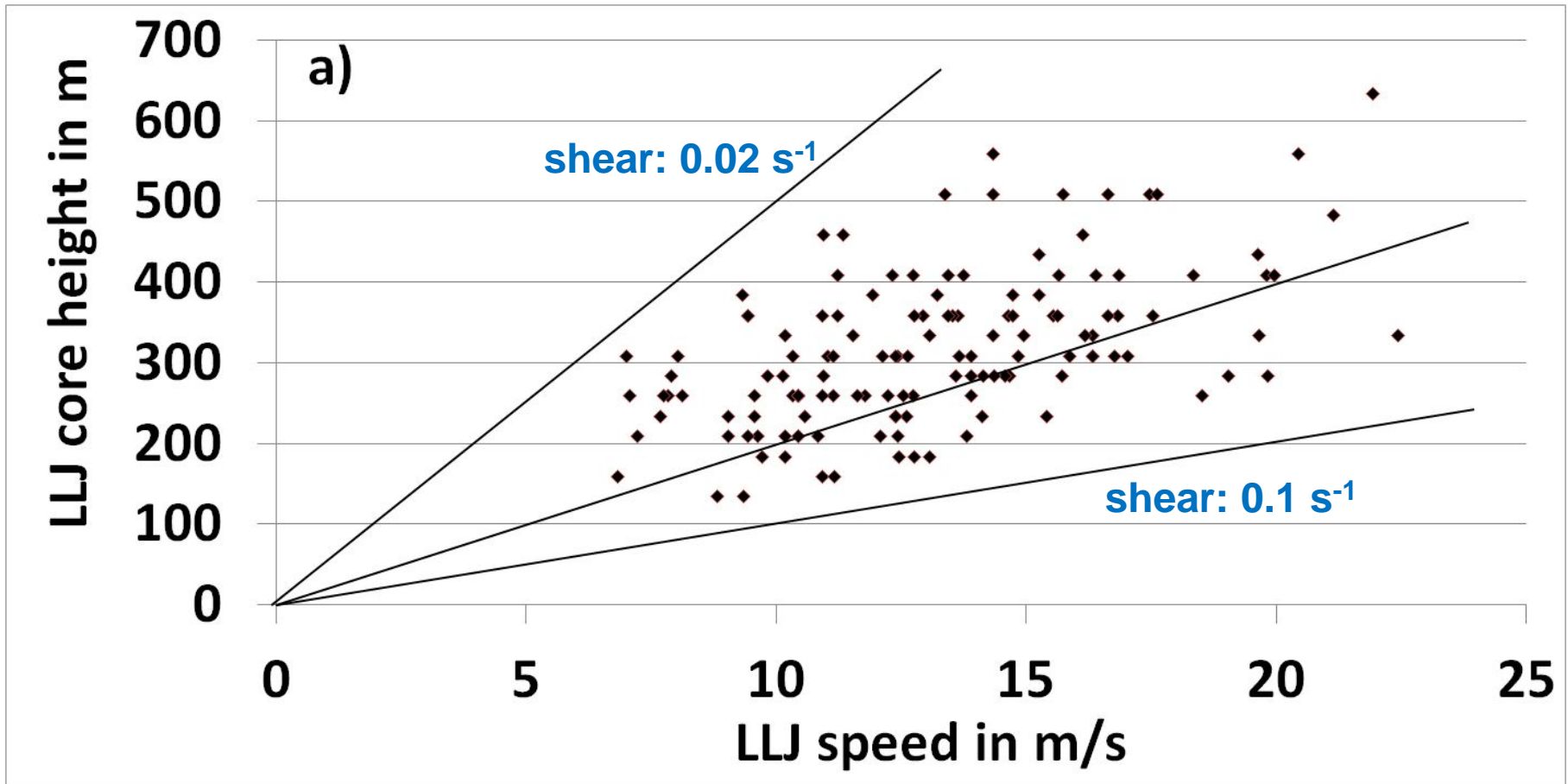
vertical profiles
of wind direction

26 June 2005

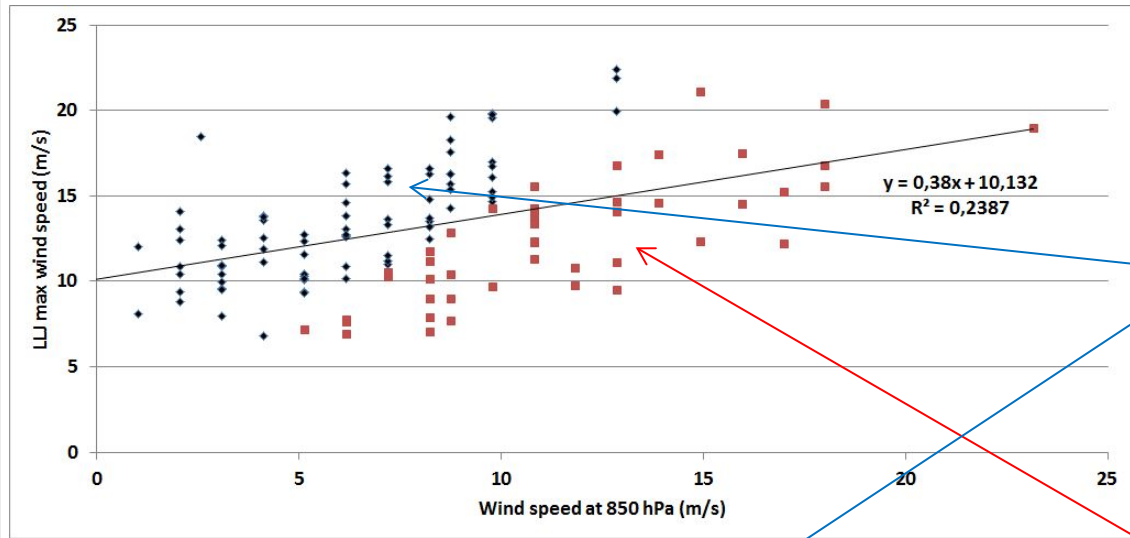
AdP Ch d G



height in m and core-speed in m/s of LLJ Hannover 5.2001 – 4.2003

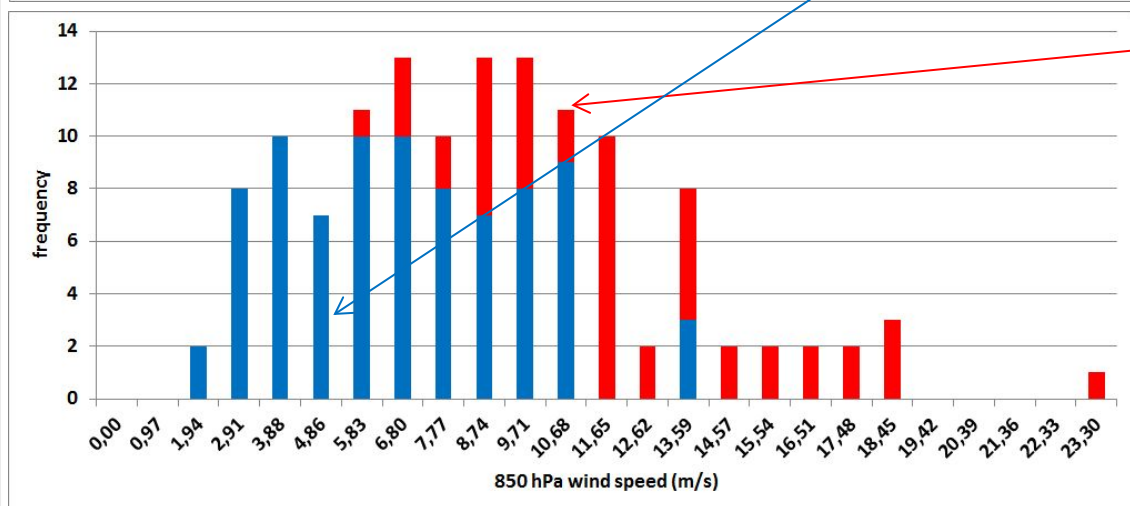


LLJ wind speed and frequency as function of 850 hPa wind speed



blue: LLJ core speed more than 1.5 times 850 hPa wind speed

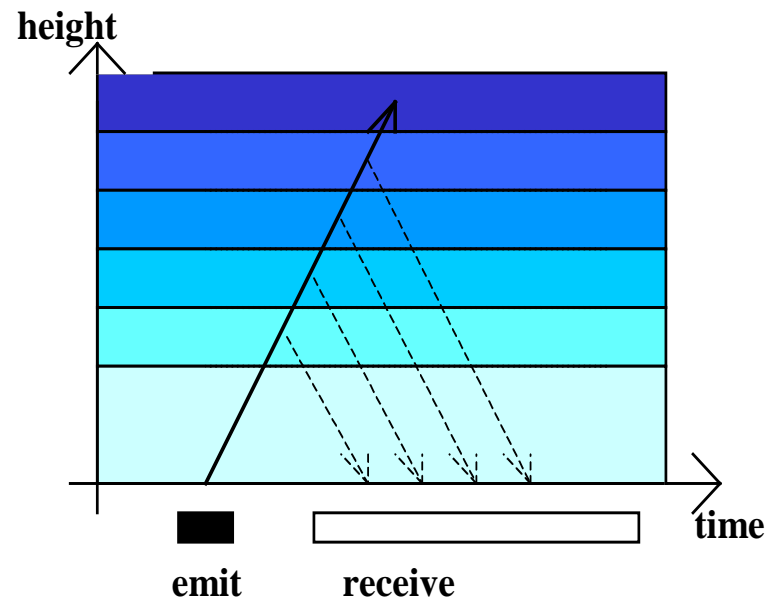
red: LLJ core speed less than 1.5 times 850 hPa wind speed



Ceilometer

**algorithms for the determination of
mixing-layer height**

Ceilometer/LIDAR measuring principle



detection:

travel time of signal	= height
backscatter intensity	= particle size and number distribution
Doppler-shift	= cannot be analyzed from ceilometer data
	(available only from a Wind-LIDAR: velocity component in line of sight)

The LIDAR equation:

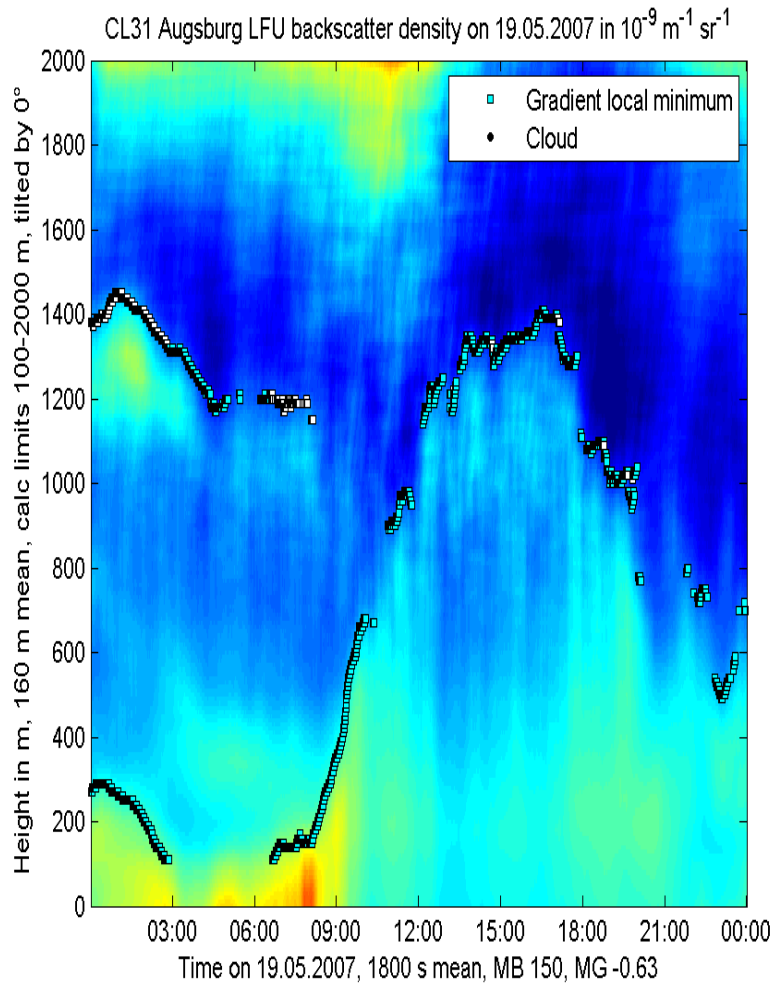
$$P_R(\lambda, r) = r^2 (c\tau A\varepsilon/2) P_0 [\beta_m(\lambda, r) + \beta_p(\lambda, r)] e^{-2\sigma r} + P_{bg}$$

- r** distance between the LIDAR and the backscattering object,
- c** speed of light,
- τ** pulse duration,
- A** antenna area,
- ε** correction term for the detector efficiency and losses due to the lenses,
- P_0** emitted energy,
- β_m** backscatter coefficient for molecules
- β_p** backscatter coefficient for particles,
- σ** absorption of light in the atmosphere,
- P_{bg}** background noise.

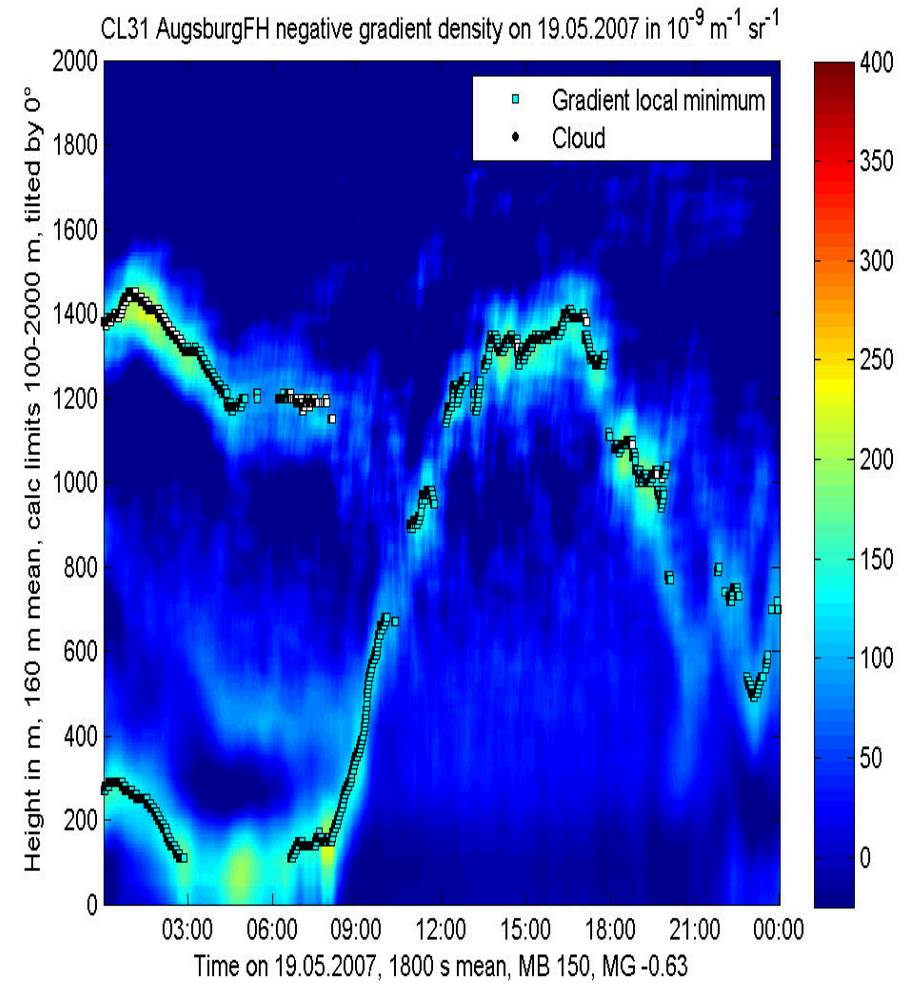
For a ceilometer β_m is negligible and only β_p is important

ceilometer sample plot (daytime convective BL)

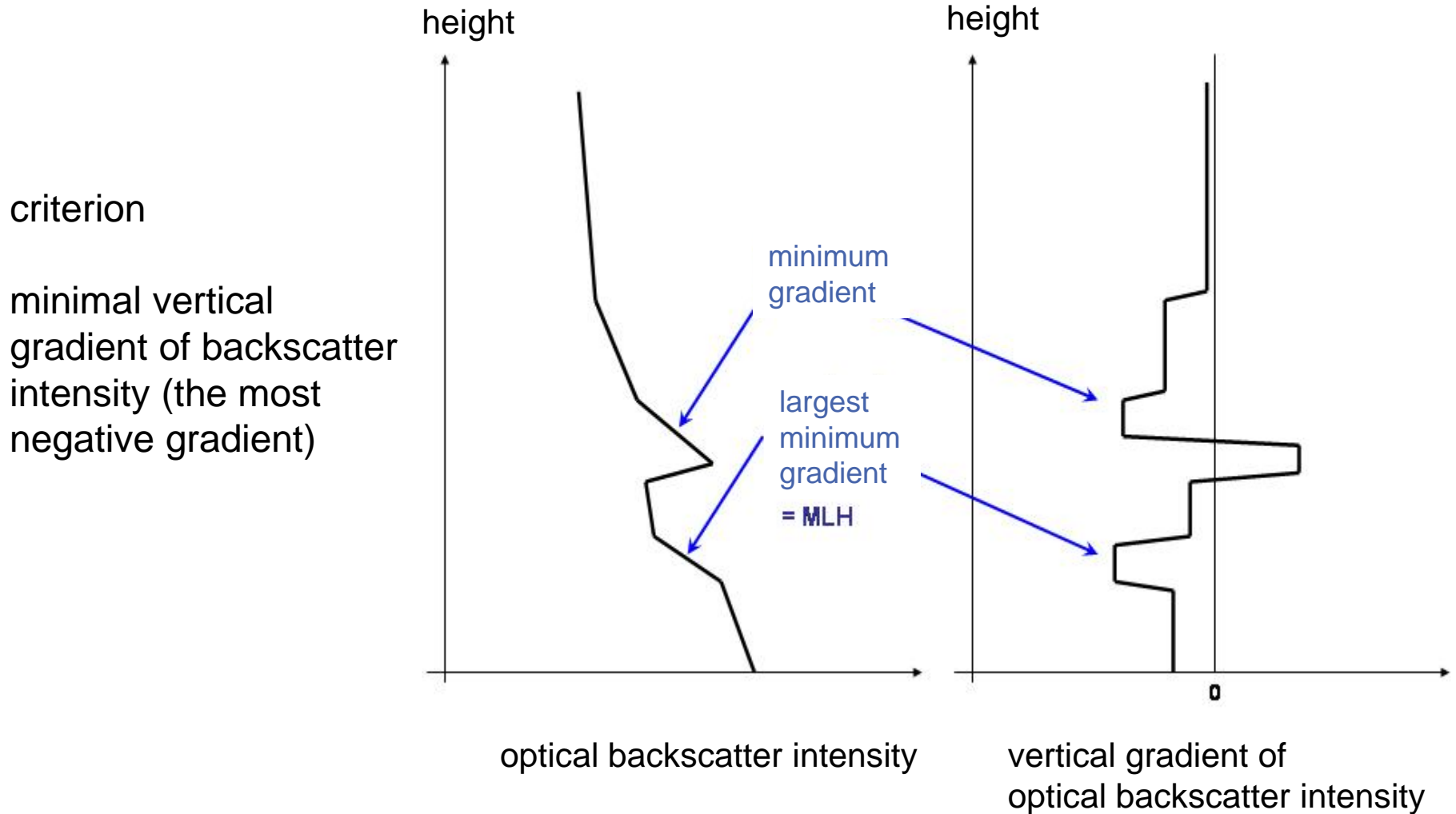
optical backscatter intensity



negative vertical gradient of optical backscatter intensity



Algorithm to detect MLH from Ceilometer-Daten

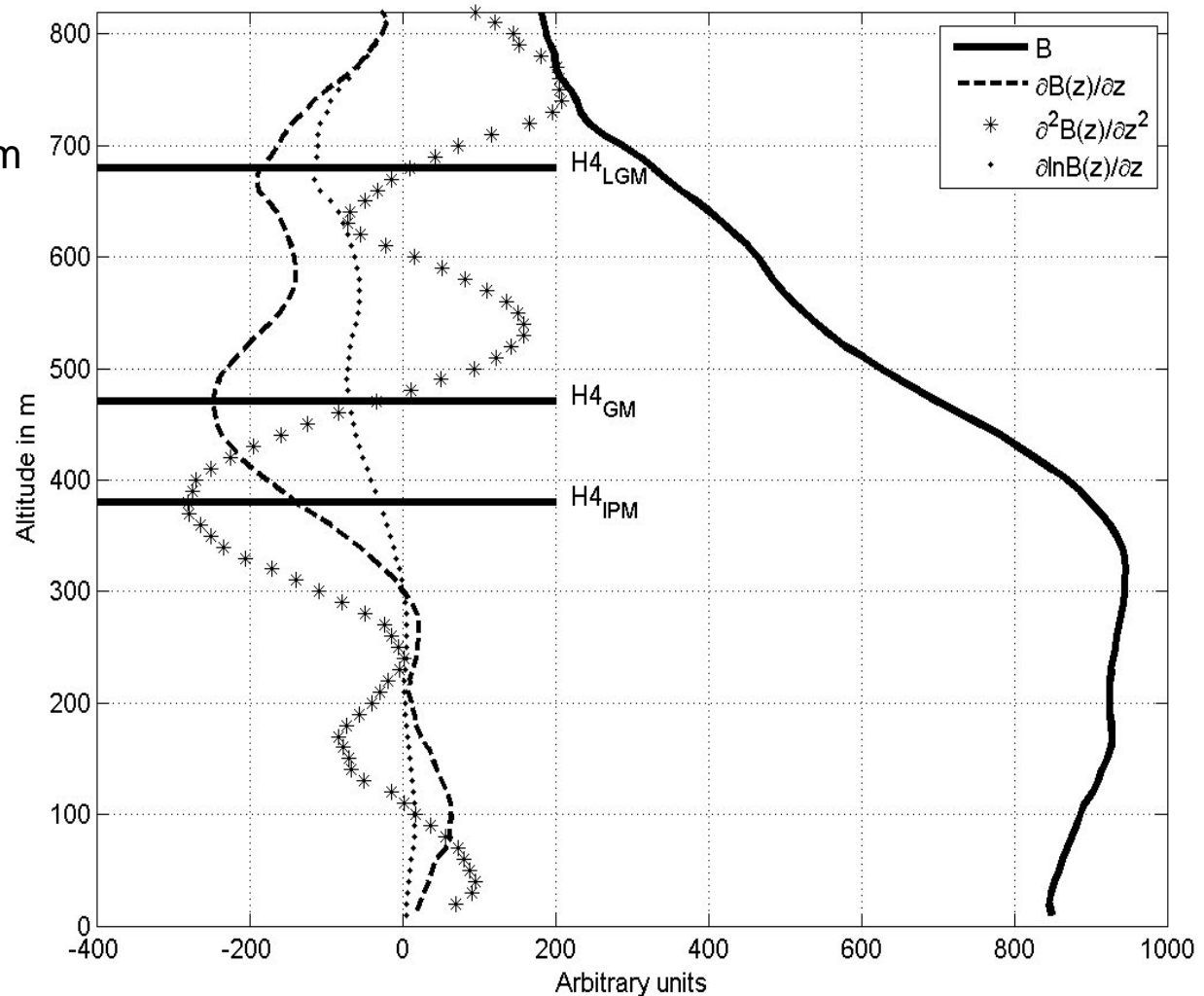


Different gradient methods (see Sicard et al. 2006, BLM 119, 135-157)

logarithmic gradient minimum

gradient minimum

inflection point method
(minimum of 2nd derivative)



comparison of two different ceilometers

LD40

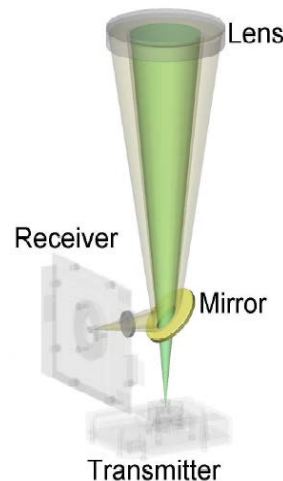
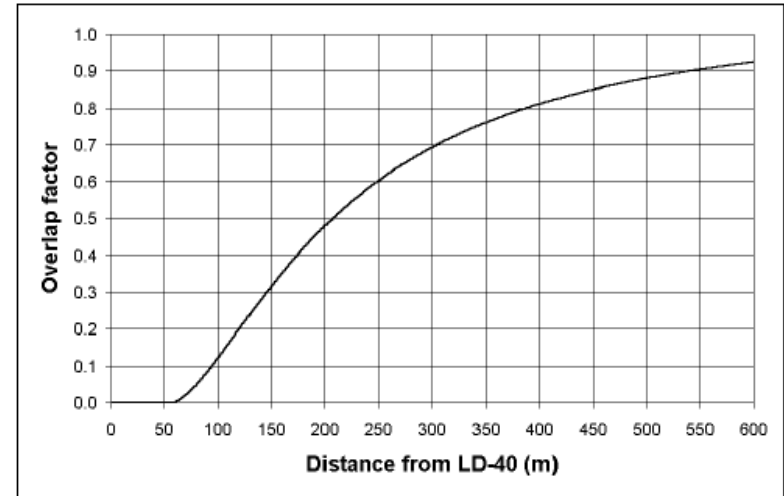
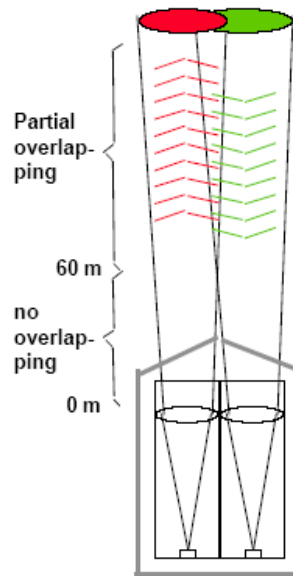
two optical axes

wave length: 855 nm
height resolution: 7.5 m
max. range: 13000 m

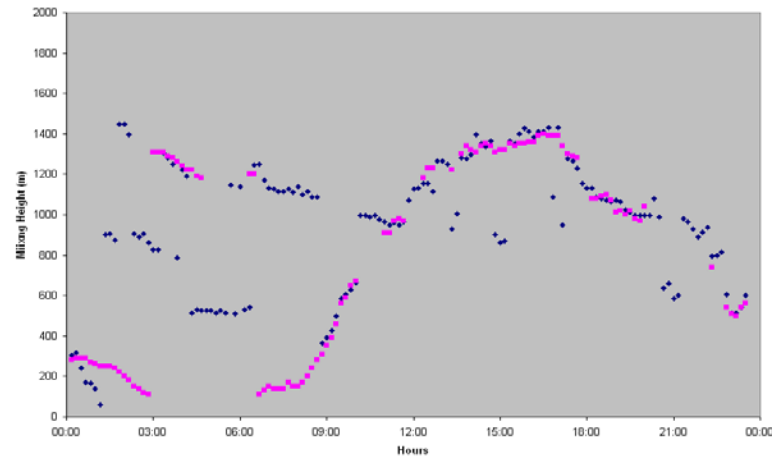
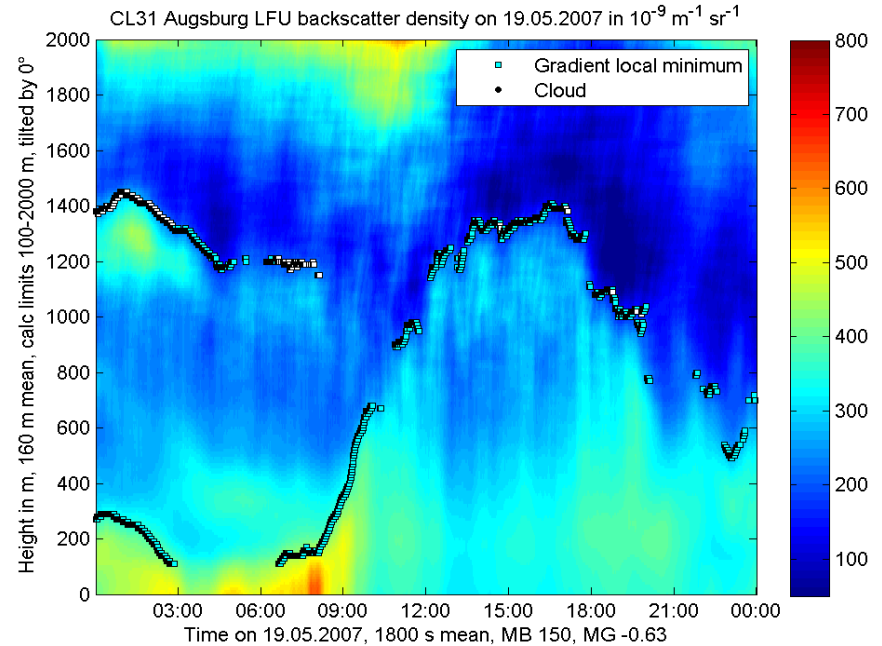
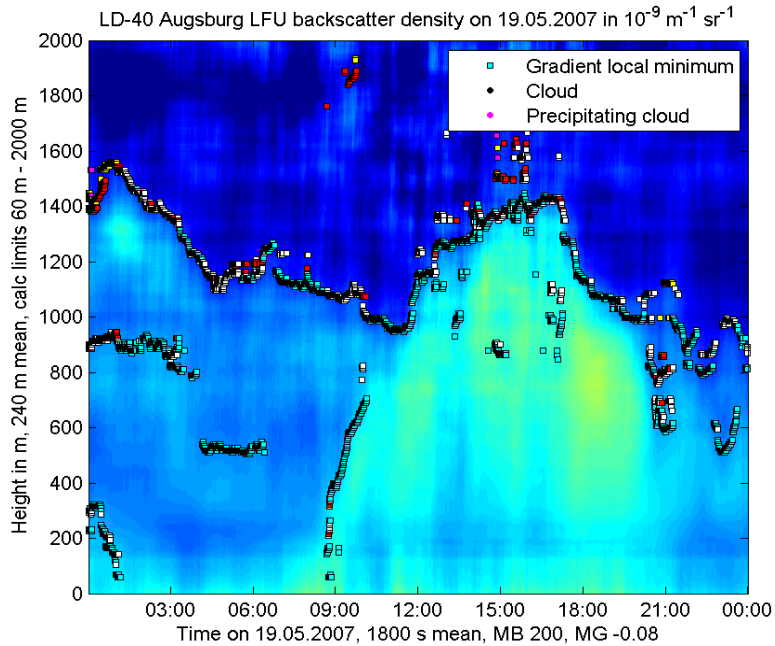
CL31 / CL51

one optical axis

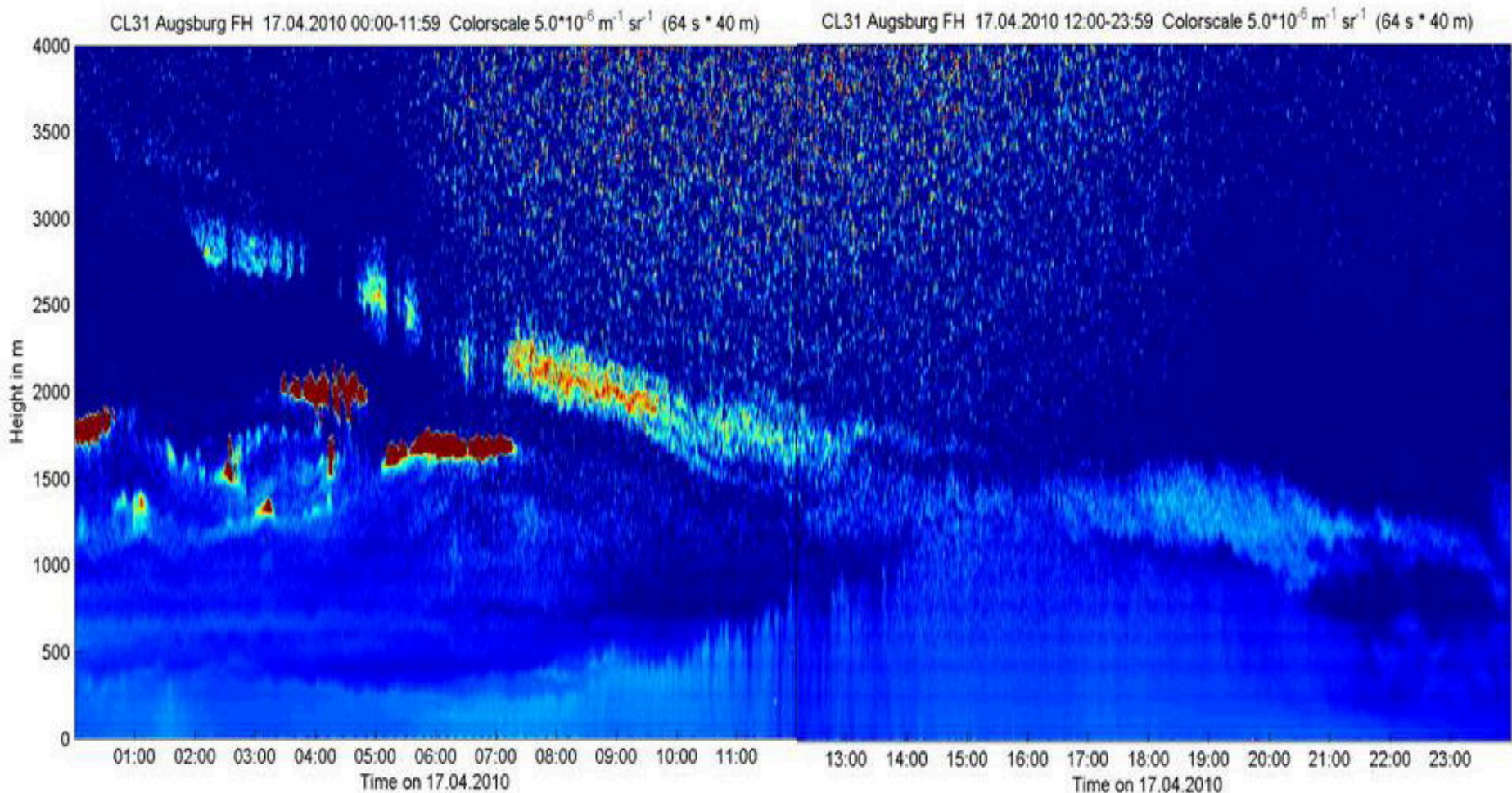
wave length: 905 nm
height resolution: 5 m
max. range: 7500 m



comparison of LD40 and CL31



Eyjafjallajökull ash cloud over Southern Germany



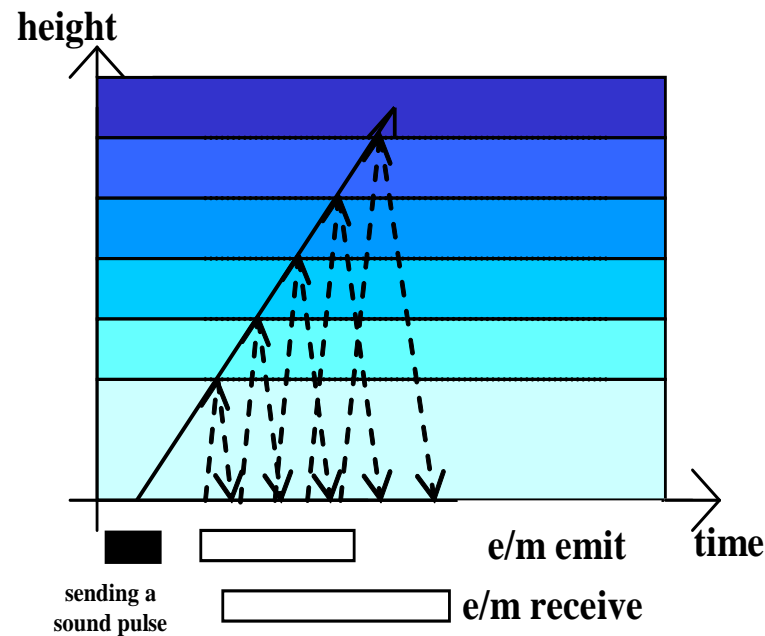
read more: Emeis, S., R. Forkel, W. Junkermann, K. Schäfer, H. Flentje, S. Gilje, W. Fricke, M. Wiegner, V. Freudenthaler, S. Groß, L. Ries, F. Meinhardt, W. Birmili, C. Münkel, F. Obleitner, P. Suppan, 2011: Measurement and simulation of the 16/17 April 2010 Eyjafjallajökull volcanic ash layer dispersion in the northern Alpine region. *Atmos. Chem. Phys.*, 11, 2689–2701

RASS

principles of operation

examples

RASS measuring principle



detection:

travel time of em./ac. signal	= height	
ac. backscatter intensity	= turbulence	(identical to SODAR)
ac. Doppler-shift	= line-of-sight wind speed	(identical to SODAR)
em. Doppler shift	= sound speed → temperature	

RASS (radio-acoustic remote sensing)

measures vertical temperature profiles

Bragg-RASS: windprofiler plus acoustic component

Doppler-RASS: SODAR plus electro-magnetic component

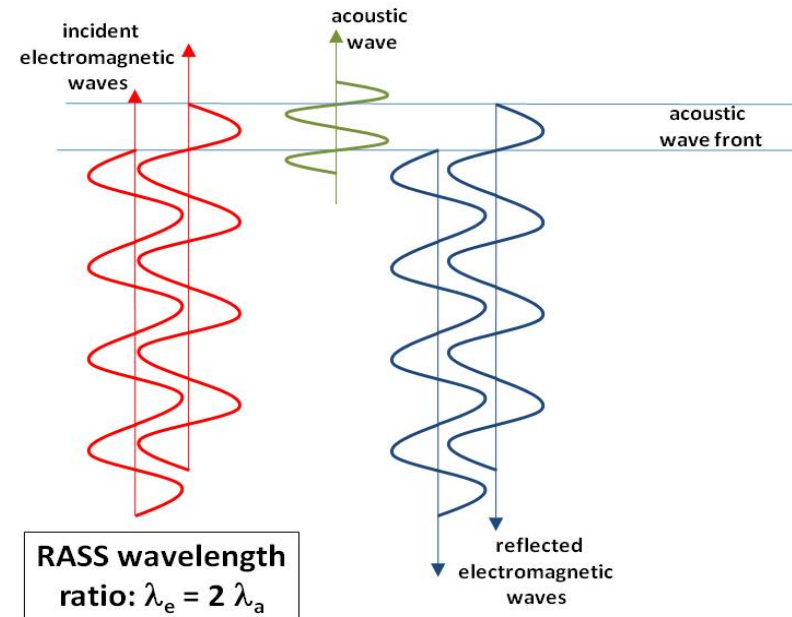
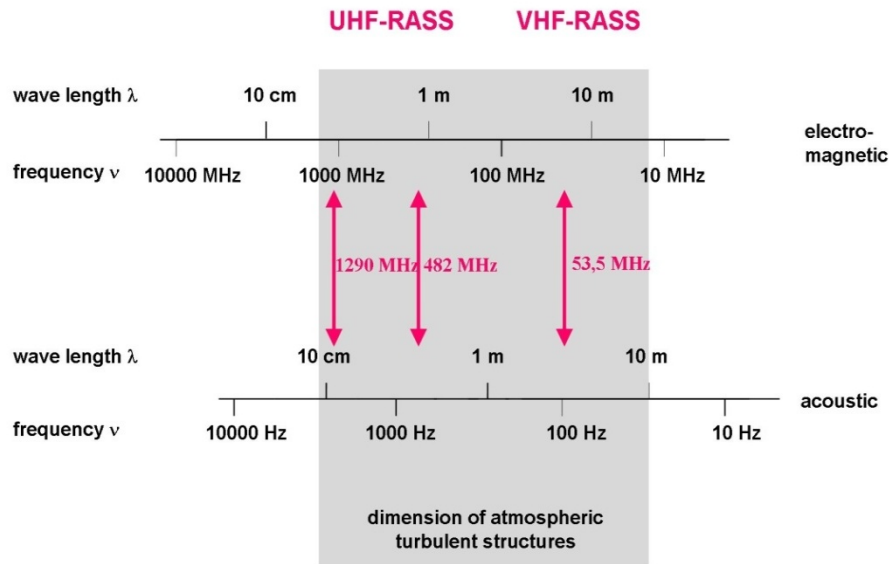
UHF RASS (boundary layer)

VHF RASS (troposphere)

RASS: frequencies

**Bragg condition:
acoustic wavelength = 1/2 electro-magnetic wavelength**

electro-magnetic - acoustic frequency pairs for RASS devices



Emeis, S., 2010: Measurement Methods in Atmospheric Sciences - In situ and remote. Borntraeger, Stuttgart, 272 pp., 103 figs, 28 tables, ISBN 978-3-443-01066-9.



SODAR-RASS (Doppler-RASS) (METEK)

acoustic frequ.: 1077 Hz

radio frequ.: 474 MHz

resolution: 20 m

lowest

range gate: ca. 40 m

vertical range: 540 m



Bragg-RASS

acoustic frequ.: about 3000 Hz

radio frequ.: 1290 MHz

resolution: 50 m

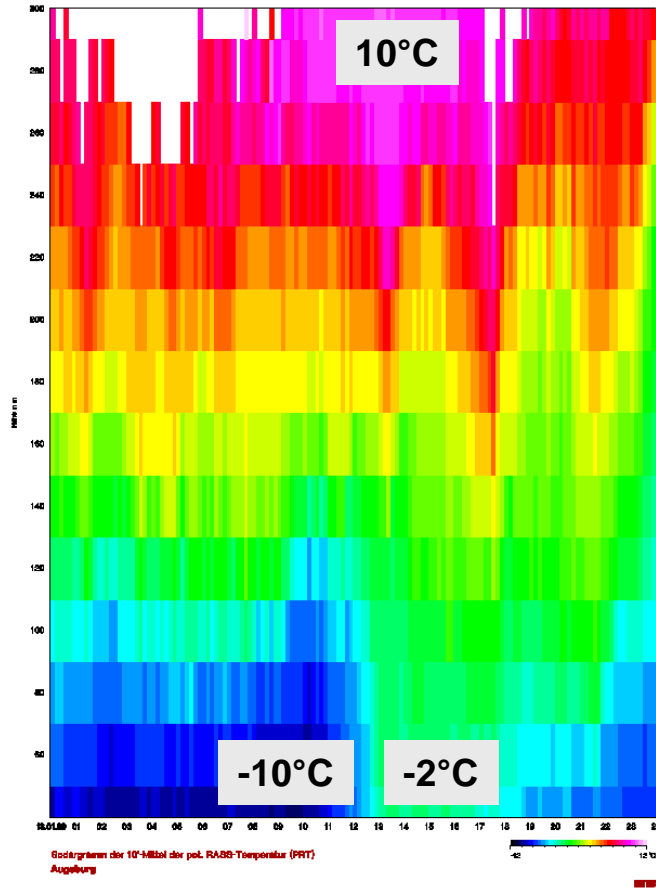
lowest

range gate: ca. 200 m

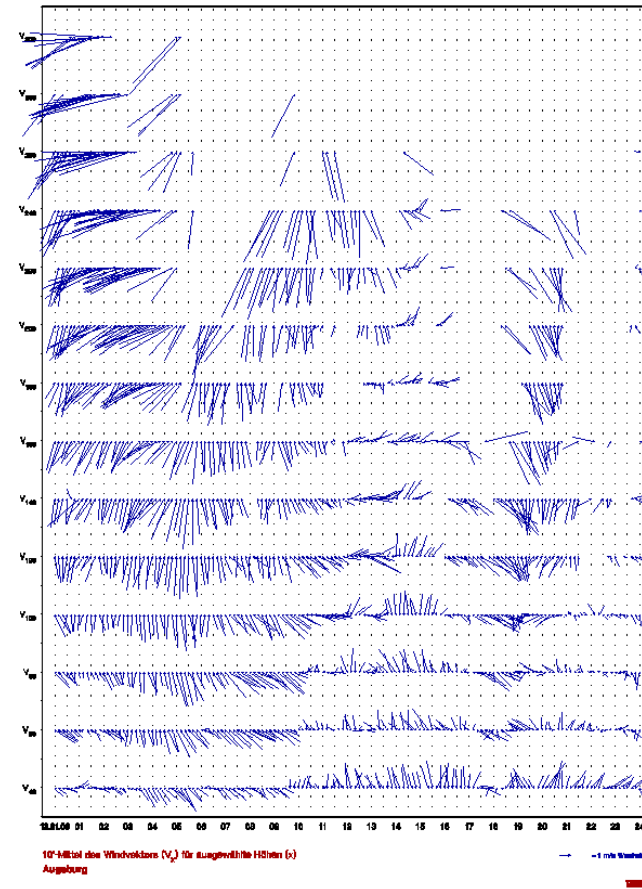
vertical range: 1000 m

example RASS data: winter day potential temperature (left), horizontal wind (right)

300 m



40 m



Critical Richardson number is limiting condition for vertical shear

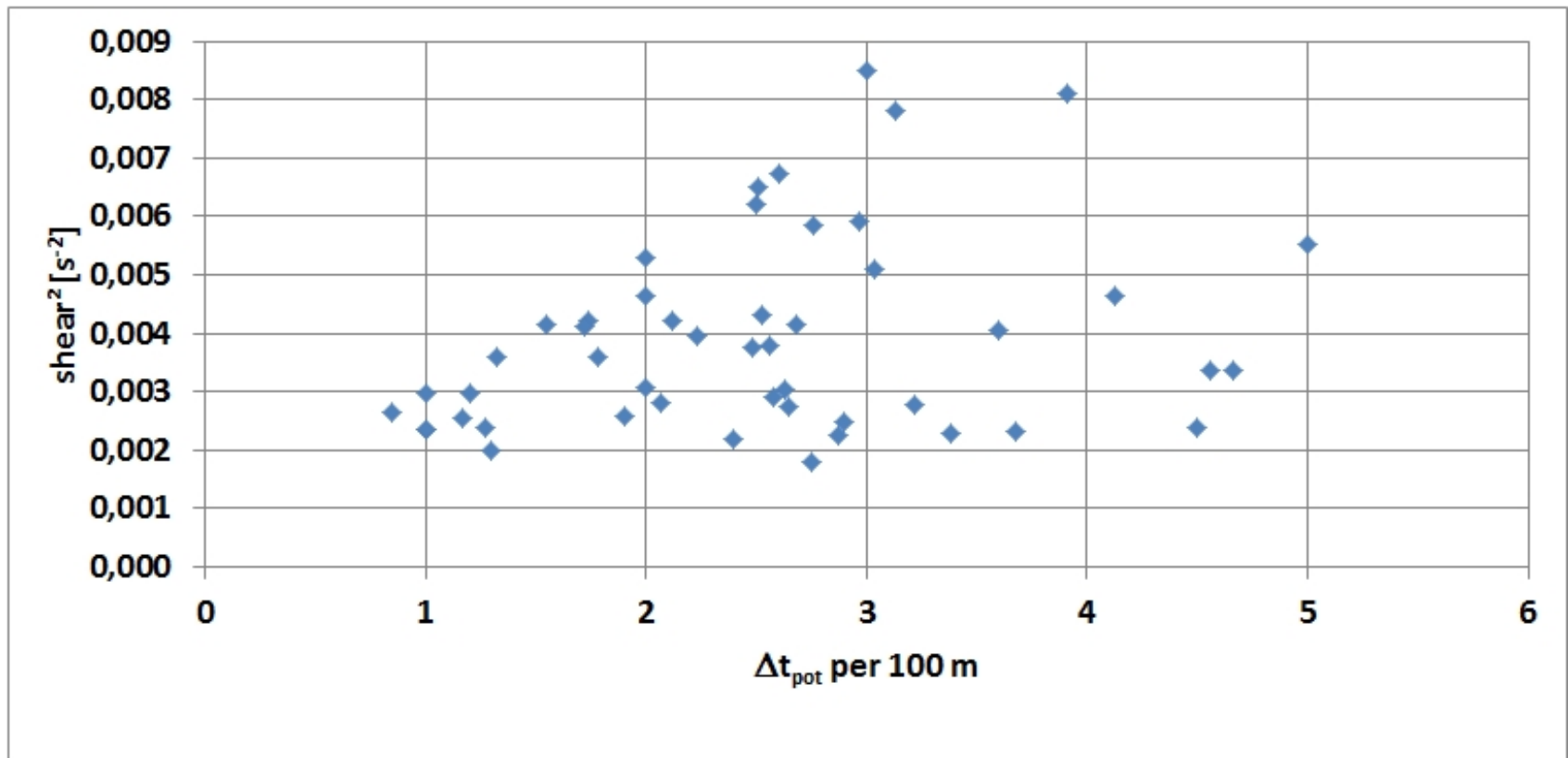
(mechanical turbulence is generated if Ri falls below Ri_{krit})

$$Ri_{krit} = \frac{g\partial\Theta/\partial z}{\Theta(\partial u/\partial z)^2} \approx 0.25$$

$\Theta(z)$	potential temperature
g	gravitational acceleration
$u(z)$	wind speed
z	vertical coordinate

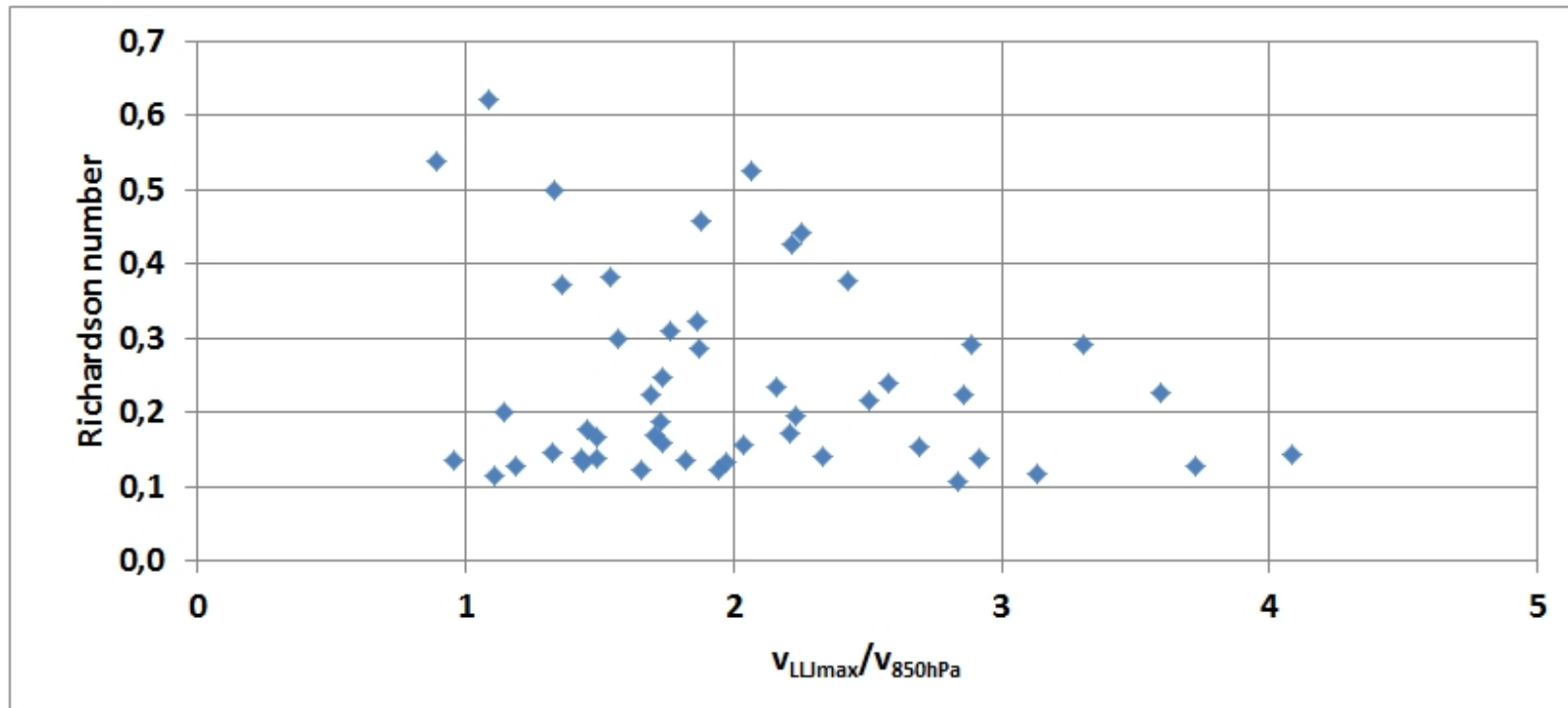
RASS observations Augsburg

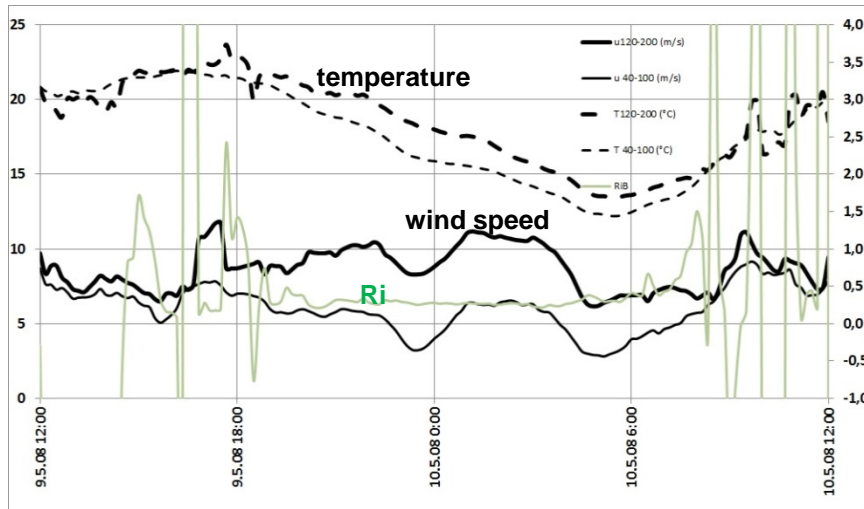
correlation between shear and temperature gradient



RASS observations Augsburg

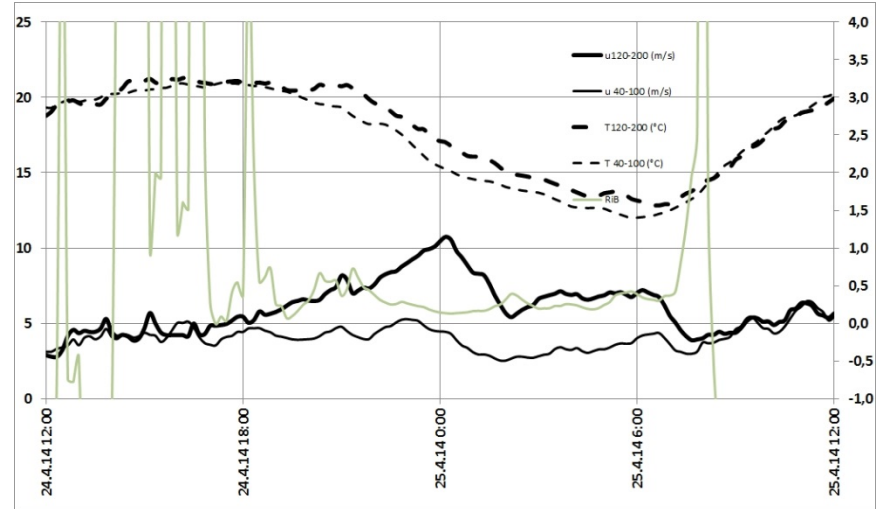
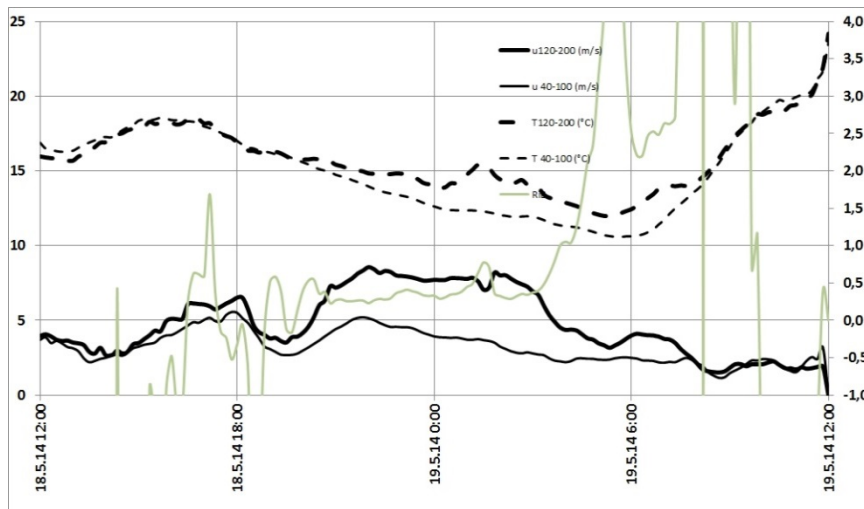
Richardson number during LLJ events



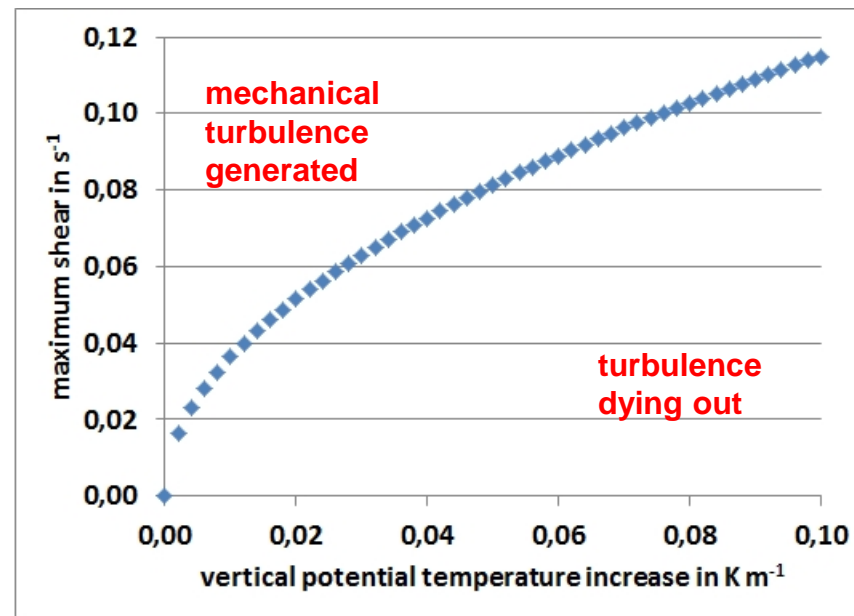


RASS observations Augsburg

critical Richardson Number
between 40 and 200 m above ground
as limiting value
for nocturnal LLJ



maximum possible shear for a given $Ri_{krit} = 0.25$

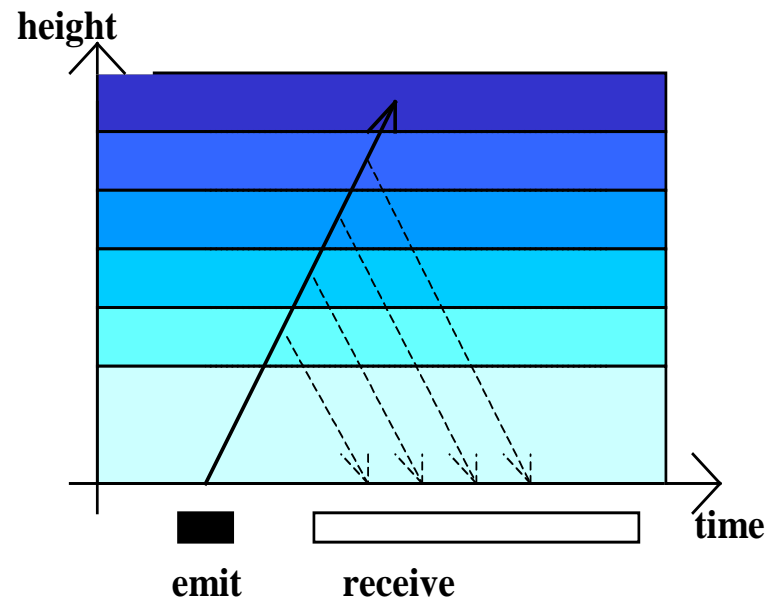


$$Ri_{krit} = \frac{g \partial \Theta / \partial z}{\Theta (\partial u / \partial z)^2} \approx 0.25$$

Doppler windlidar

**wind, turbulence, aerosol detection,
mixing-layer height, low-level jet**

Doppler windlidar measuring principle



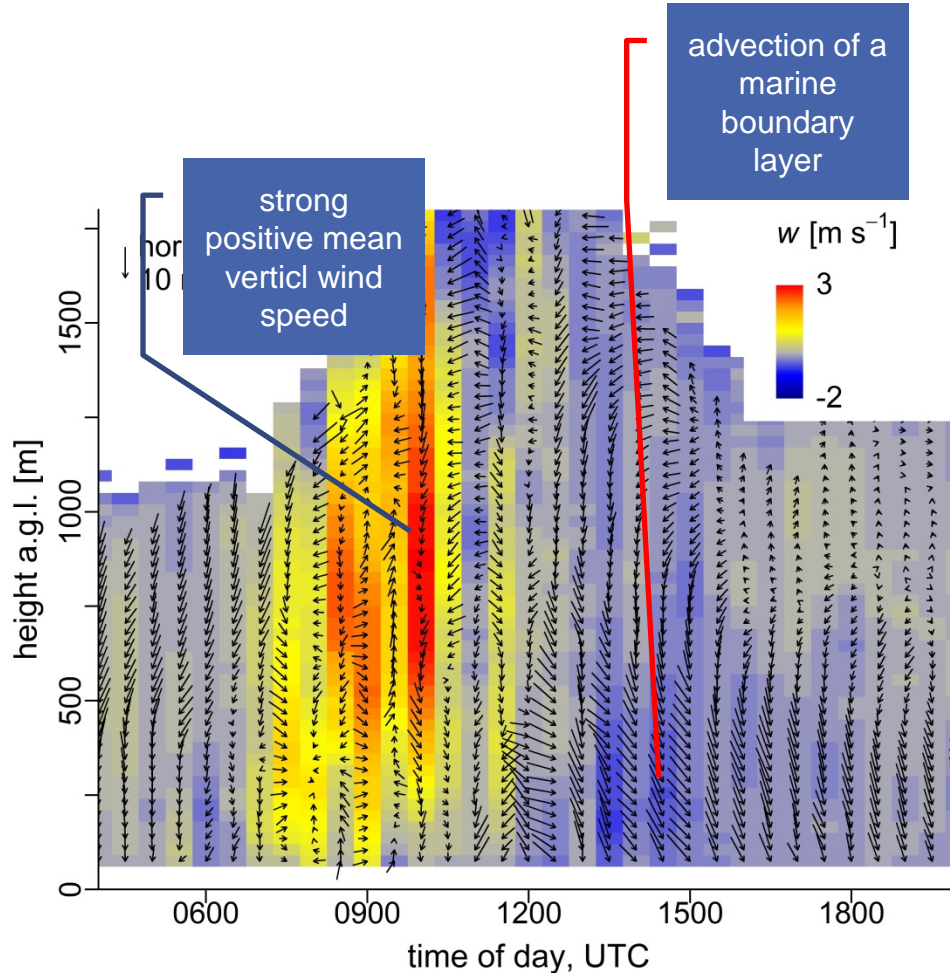
detection:

travel time of signal	= height
backscatter intensity	= particle size and number distribution
depolarisation	= particle shape
Doppler-shift	= wind speed in the line of sight

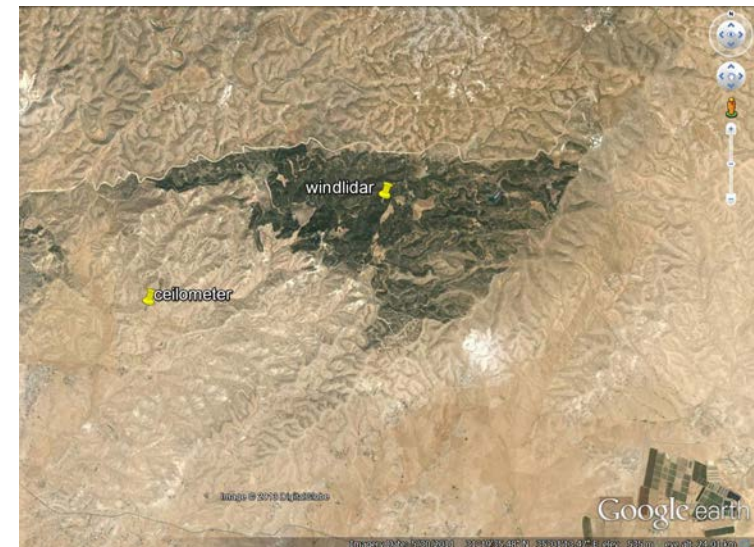
mobile Doppler windlidar from Halo Photonics



Yatir Forest, Israel



The 3-d wind field above the Yatir forest on 10 Sept 2013. The colour indicates the vertical wind component. The white arrows indicate the horizontal wind component: the direction of the arrow shows the wind direction, the length of the arrow shows the wind speed. During the afternoon hours, there is a 180°-shift in wind direction between surface and boundary-layer top which indicates a stationary circulation. Please note that this picture is not shown in local time, but in UTC (i.e. 12:00 means 14:00 Israel winter time)

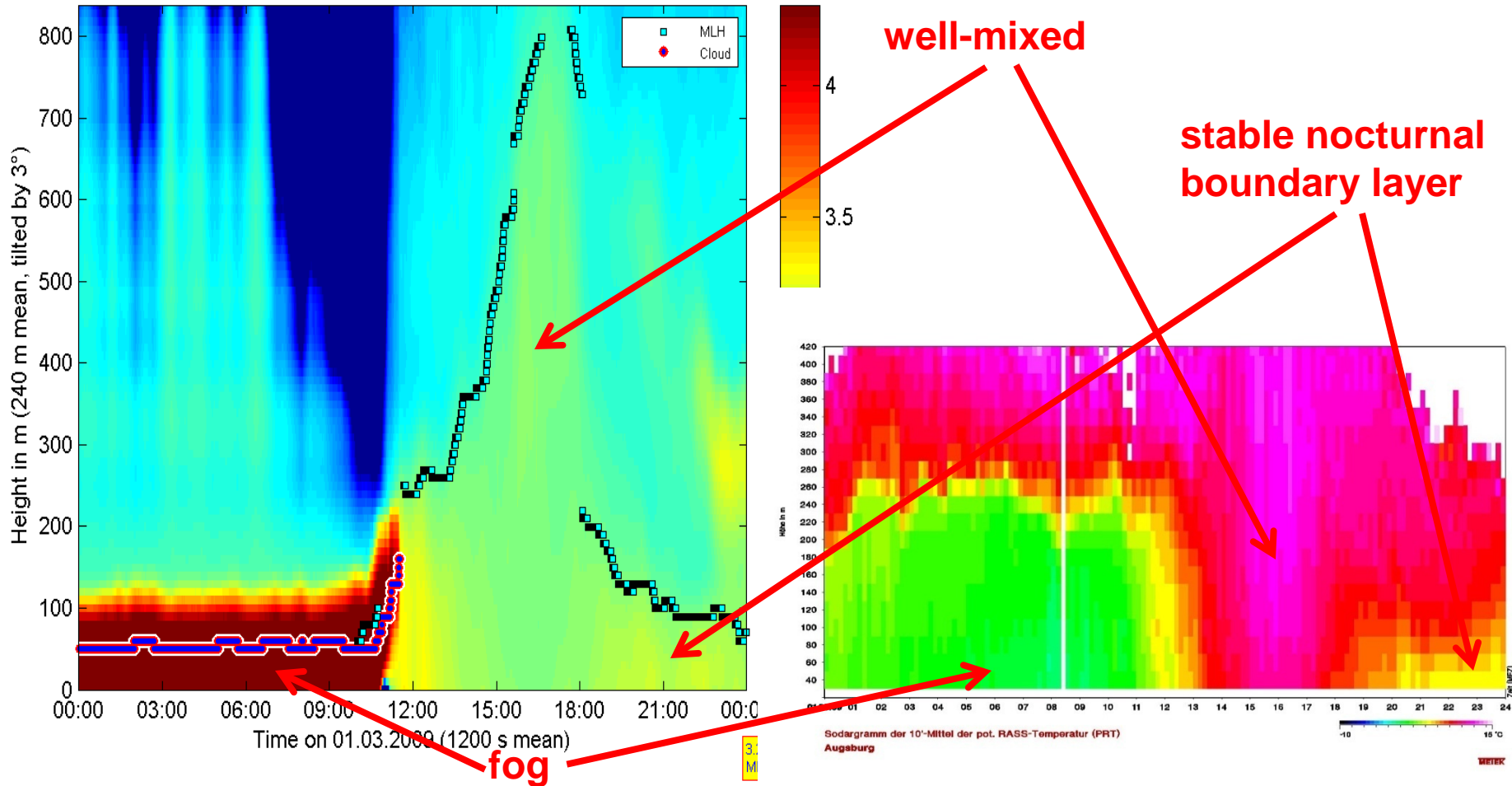


(Eder and Mauder, IMK-IFU (KIT), personal communication)

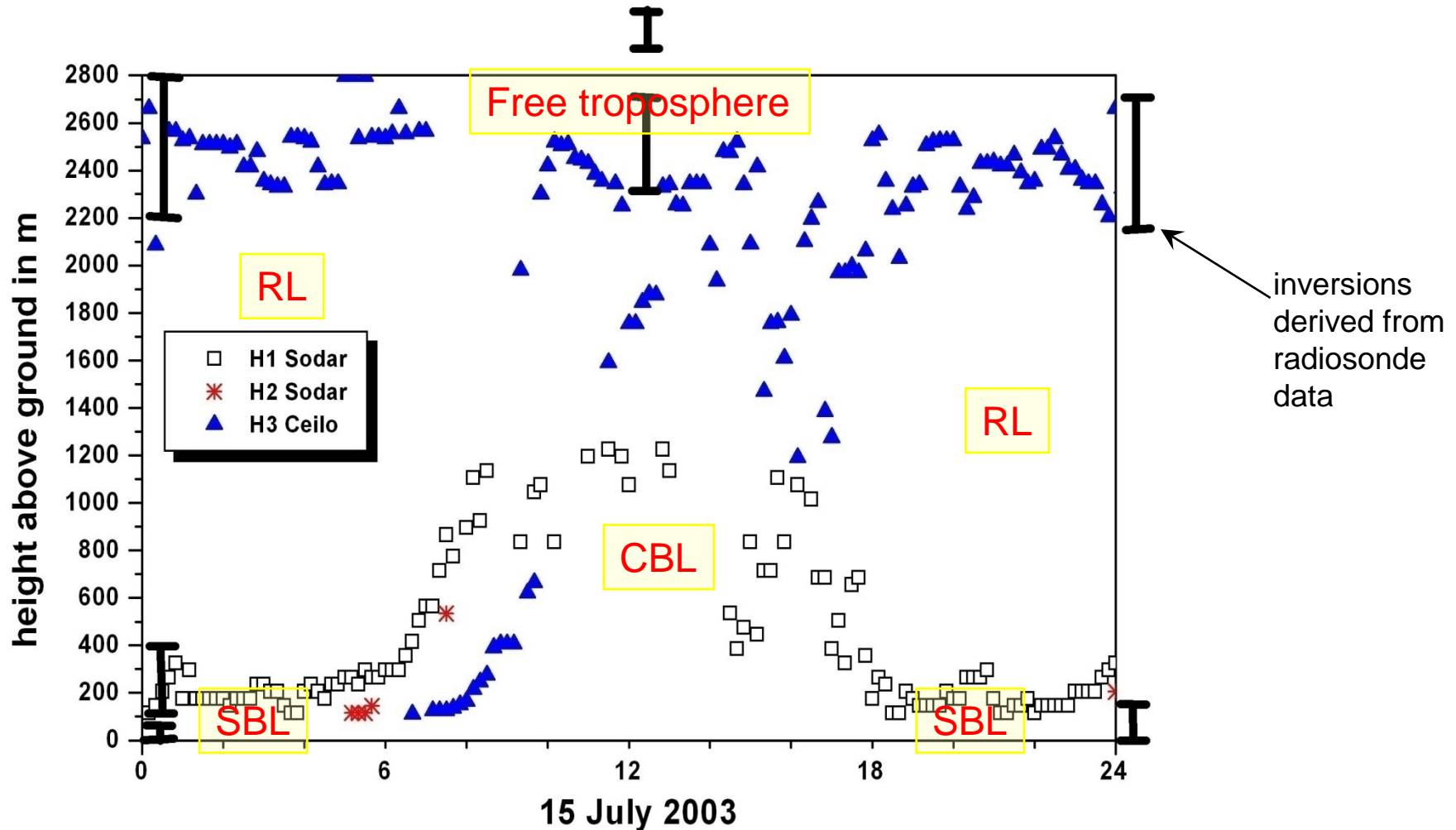
Comparisons between different instruments

comparison of RASS data (potential temperature, right) with aerosol backscatter from a ceilometer (left)

CL31 Augsburg AVA log₁₀ of backscatter with MLH on 01.03.2009 in 10⁻⁹ m⁻¹ sr⁻¹

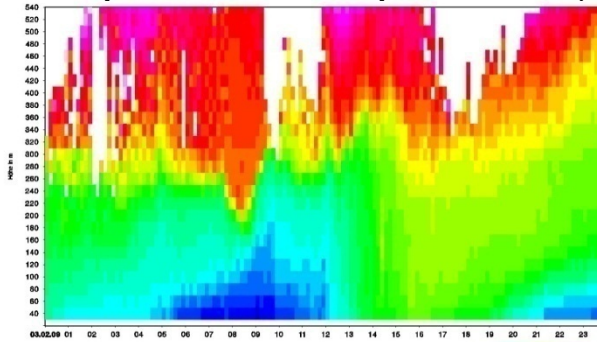


Differences in MLH detection from SODAR and Ceilometer data taken in Budapest

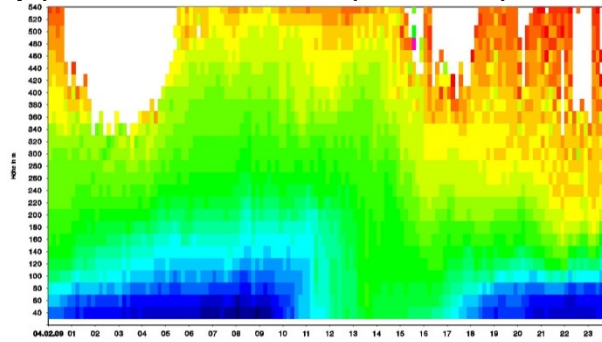


Emeis, S., K. Schäfer, 2006: Remote sensing methods to investigate boundary-layer structures relevant to air pollution in cities. *Bound.-Lay Meteorol.*, 121, 377-385,

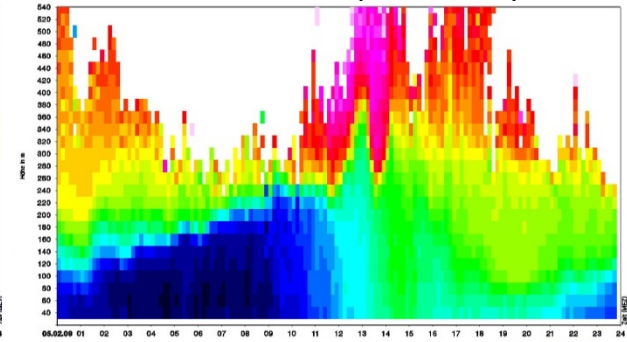
potential temperature (top), MLH RASS (middle), MHL SODAR/Ceilo (bottom)



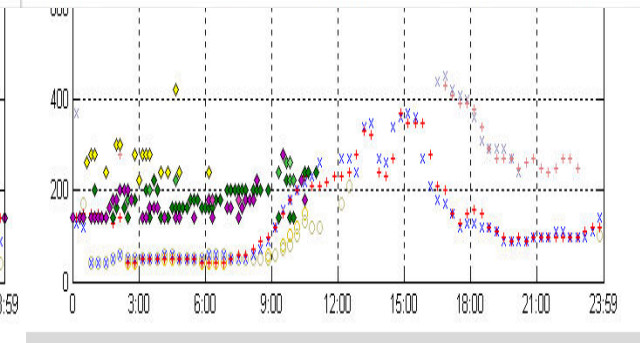
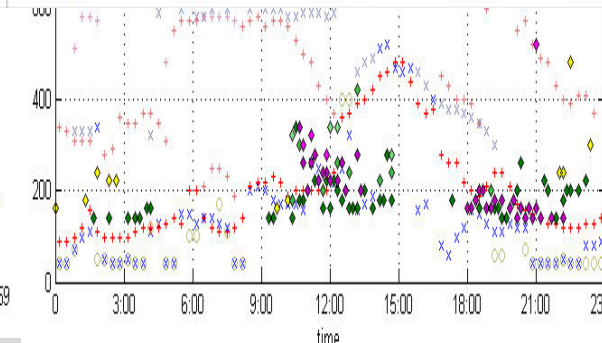
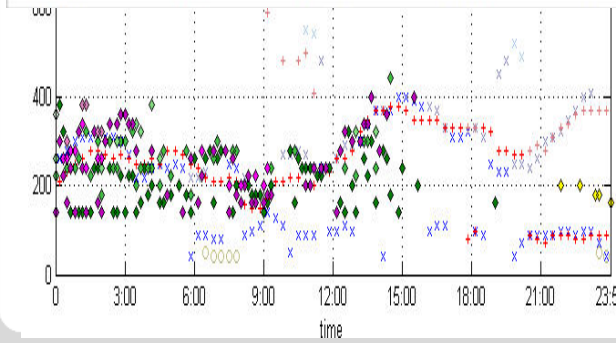
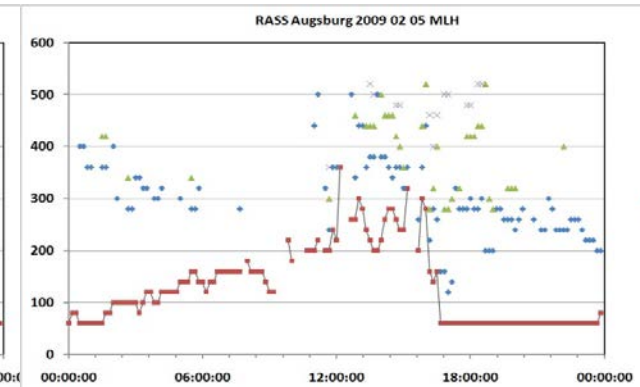
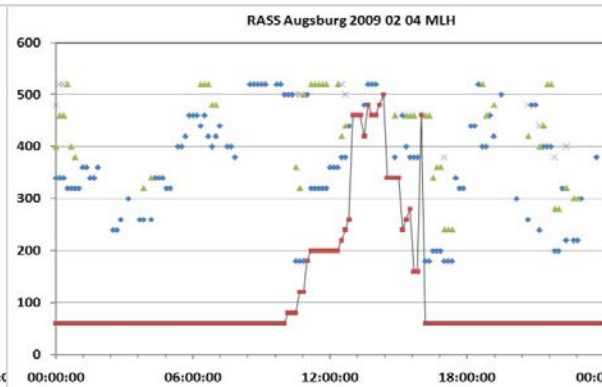
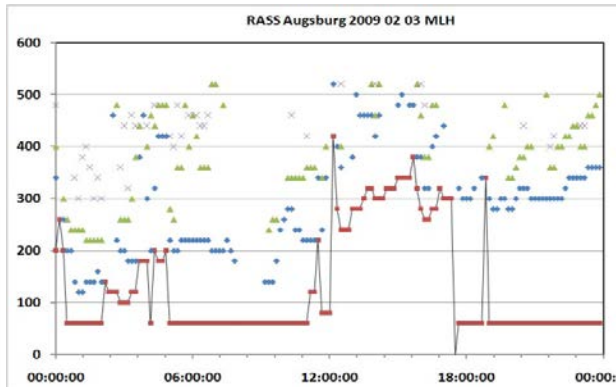
Feb. 3



Feb. 4



Feb. 5



Summary

Clicker question:

Which instrument is best?

- A sodar**
- B ceilometer**
- C wind lidar**
- D RASS**
- E don't know**

quality criteria:

data availability

vertical range

direct/indirect detection

Doppler analysis

😊😊😊💧* **RASS** delivers temperature profiles, wind profiles are additionally available.
MLH directly from temperature profiles. LLJ from wind profiles.
Does not work properly under high wind speeds. Restricted range.

😊😊😊💧* **wind lidar** detects wind profiles, aerosol distribution and water droplets.
It has to be assumed that the aerosol follows the thermal structure of the atmosphere and the wind.
MLH from aerosol backscatter, wind speed variance, LLJ from wind profiles.
Does not work properly in extreme clear (aerosol-free) air and during precipitation events and fog.

😊😊😊💧*💧* **Ceilometer** detects aerosol distribution and water droplets. It has to be assumed that the aerosol follows the thermal structure of the atmosphere.
MLH indirectly from aerosol backscatter using a MLH algorithm.
Does not work properly in extreme clear (aerosol-free) air and during precipitation events and fog.

😊💧*💧*💧* **SODAR** detects wind profiles, temperature fluctuations and gradients, but no absolute temperature.
MLH indirectly from acoustic backscatter (MLH algorithm). LLJ from wind profiles.
Does not work properly under perfectly neutral stratification, with very high wind speeds, and during stronger precipitation events. Restricted range.

Literature

Asimakopoulos, D.N., C.G. Helmis, J. Michopoulos, 2004: Evaluation of SODAR methods for the determination of the atmospheric boundary layer mixing height. - Meteor. Atmos. Phys. 85, 85–92.

Beyrich, F., 1997: Mixing height estimation from sodar data – a critical discussion. - Atmos. Environ. 31, 3941–3953.

Ceilometer:

Schäfer, K., S.M. Emeis, A. Rauch, C. Münkel, S. Vogt, 2004: Determination of mixing-layer heights from ceilometer data. In: Remote Sensing of Clouds and the Atmosphere IX. Schäfer, K., A. Comeron, M. Carleer, R.H. Picard, N. Sifakis (Eds.), Proc. SPIE, Bellingham, WA, USA, Vol. 5571, 248–259.

Sicard, M., C. Pérez, F. Rocadenbosch, J.M. Baldasano, D. García-Vizcaino, 2006: Mixed-Layer Depth Determination in the Barcelona Coastal Area From Regular Lidar Measurements: Methods, Results and Limitations. - Bound.-Lay. Meteor. 119, 135–157.

RASS:

Engelbart, D.A.M., J. Bange, 2002: Determination of boundary-layer parameters using wind profiler/RASS and sodar/RASS in the frame of the LITFASS project. Theor. Appl. Climatol. 73, 53–65.

Emeis, S., K. Schäfer, C. Münkel, 2009: Observation of the structure of the urban boundary layer with different ceilometers and validation by RASS data. Meteorol. Z., 18, 149-154. **(Open access, freely available from <http://dx.doi.org/10.1127/0941-2948/2009/0365>)**

Emeis, S., K. Schäfer, C. Münkel, R. Friedl, P. Suppan, 2011: Evaluation of the interpretation of ceilometer data with RASS and radiosonde data. Bound.-Lay. Meteorol., online April 5, 2011. DOI: [10.1007/s10546-011-9604-6](https://doi.org/10.1007/s10546-011-9604-6)

Windlidar:

Emeis, S., M. Harris, R.M. Banta, 2007: Boundary-layer anemometry by optical remote sensing for wind energy applications. - Meteorol. Z., 16, 337-347.

Low-level jets:

Emeis, S., 2014: Wind speed and shear associated with low-level jets over Northern Germany. Meteorol. Z., 23, 295-304. DOI: 10.1127/0941-2948/2014/0551 ([Open Access](#))

Reviews:

Emeis, S., K. Schäfer, C. Münkel, 2008: Surface-based remote sensing of the mixing-layer height – a review. - Meteorol. Z., 17, 621-630. DOI: 10.1127/0941-2948/2008/0312 ([Open access](#))

Emeis, S., 2014: Current issues in wind energy meteorology. Meteorol. Appl., 21, 803-819. DOI: 10.1002/met.1472

Emeis, S., 2015: Observational techniques to assist the coupling of CWE/CFD models and meso-scale meteorological models. J. Wind Eng. Industr. Aerodyn., in print. DOI: 10.1016/j.jweia.2015.04.018

Books:

Wind energy meteorology

Emeis, S., 2012: Wind Energy Meteorology - Atmospheric physics for wind power generation. Springer Heidelberg etc., XIV+196 pp. ISBN 978-3-642-30522-1, DOI 10.1007/978-3-642-30523-8

Chinese Edition: 国际电气工程先进技术译丛: 风能气象学 (Guo ji dian qi gong cheng xian jin ji shu yi cong: Feng neng qi xiang xue), China Machine Press Advanced Technology of Electrical Engineering International Translations, ISBN: 978-7-111-44668-2

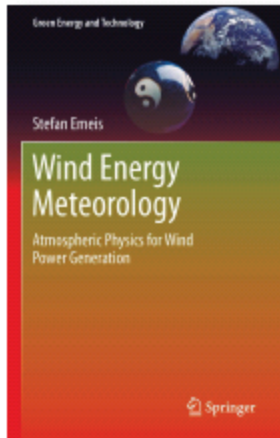
boundary-layer remote sensing with application examples:

Emeis, S., 2011: Surface-Based Remote Sensing of the Atmospheric Boundary Layer. Series: Atmospheric and Oceanographic Sciences Library, Vol. 40. Springer Heidelberg etc., X+174 pp. 114 illus., 57 in color., H/C. ISBN 978-90-481-9339-4, DOI 10.1007/978-90-481-9340-0

overview on the entire range of meteorological measurement methods:

Emeis, S., 2010: Measurement Methods in Atmospheric Sciences. In situ and remote. Series: Quantifying the Environment Vol. 1. Borntraeger Stuttgart. XIV+257 pp., 103 Figs, 28 Tab. ISBN 978-3-443-01066-9.

**Thank you very
much for your
attention**



2013, 2013, XIV, 196 p. 94 illus., 16 in color.

 **Printed book**

Hardcover

- ▶ **99,95 € | £90.00 | \$129.00**
- ▶ ***106,95 € (D) | 109,95 € (A) | CHF 133.50**

S. Emeis, Karlsruher Institut für Technologie, Garmisch-Partenkirchen, Germany
Wind Energy Meteorology

Atmospheric Physics for Wind Power Generation

- ▶ **First book devoted solely to the meteorological basics of wind power generation**
- ▶ **Presents the meteorological basics for large wind turbines and wind parks**
- ▶ **Gives guidance to plan offshore wind parks**

This book is intended to give an introduction into the meteorological boundary conditions for power generation from the wind, onshore and offshore. It is to provide reliable meteorological information for the planning and running of this important kind of renewable energy. This includes the derivation of wind laws and wind profile descriptions, especially those above the logarithmic surface layer. Winds over complex terrain and nocturnal low-level jets are considered as well. A special chapter is devoted to the efficiency of large wind parks and their wakes.

